Nano Research

ISSN 1998-0124 CN 11-5974/O4
https://doi.org/10.1007/s12274-024-6788-x

Review Article

Synthesis and modification of nanowires anchored on electrodes for electrochemical and electrophysical applications

Feiyang Mo[1], Zhitao Chen[2], Nian Liu[2] (✉), and Xing Xie[1] (✉)

[1] School of Civil and Environmental Engineering, Georgia Institute of Technology, 311 Ferst Drive NW, Atlanta, GA 30332, USA
[2] School of Chemical and Biomolecular Engineering, Georgia Institute of Technology, 311 Ferst Drive NW, Atlanta, GA 30332, USA

Received: 12 April 2024 / **Revised:** 22 May 2024 / **Accepted:** 26 May 2024

ABSTRACT

The integration of nanowires onto electrode surfaces marks a significant advancement over traditional electrode materials, conferring upon nanowire-modified electrodes a vast array of applications within electrochemical and electrophysical domains. The nanowires used for electrode modification can be catalogized into two distinct types: anchored nanowires and free-standing nanowires. A critical advantage of anchored nanowires lies in their enhanced electrical connectivity with the substrate, which reduces electrode resistance and facilitates charge transport. Furthermore, the anchorage of nanowires onto electrodes provides additional mechanical support, bolstering the structural stability of the nanowire assembly. Here, we review the development of anchored nanowires designed for applications in energy storage, electrocatalysis, and electric field treatment (EFT) over the past decade. We focus on the synthesis and modification strategies employed for anchored nanowires, culminating in the evaluation of these fabrication and enhancement techniques. Through this analysis, we aim to furnish comprehensive insights into the preparation of anchored nanowires, guiding the selection of appropriate fabrication processes and subsequent functional modifications.

KEYWORDS

electrode modification, direct growth, etching, energy storage, electrocatalysis, electric field treatment

1 Introduction

Over recent decades, one-dimensional nanostructures, including nanowires, nanobelts, nanorods, and nanofibers, have captivated significant interest due to their distinctive characteristics derived from their nanoscale dimensions [1–5]. These characteristics include high aspect ratios and extensive surface areas, enabling these structures to find diverse applications in everything from optoelectronic devices to energy storage domains [6–10]. Notably, nanowires have emerged as a focal point within one-dimensional nanostructures due to their customizable electronic, optical, and mechanical properties, which make them an exemplary platform for integration with electrodes [9–13]. The melding of nanowires with electrode surfaces introduces several benefits beyond those offered by traditional electrode materials. By exploiting the large surface-to-volume ratio of nanowires, the active surface area of electrodes can be substantially augmented, thereby enhancing the loading of active materials or catalysts [14–17]. By exploiting the high aspect ratio of nanowires, the electric field proximal to the nanowire tips can be exponentially intensified, offering substantial advantages for applications like electroporation and biological transfection [18–21]. Moreover, the intrinsic electrical conductivity of certain nanowire materials, such as metal and conductive polymer nanowires, facilitates efficient charge transport across the electrode-electrolyte interface, reducing ohmic losses and elevating the overall electrochemical performance [22–25].

Electrodes modified with nanowires demonstrate extensive utility in electrochemical and electrophysical domains, with one of the most notable applications in energy storage solutions, particularly lithium-ion batteries (LIBs) [10, 26]. For instance, silicon nanowire-modified electrodes, serving as anodes, are rigorously explored for their superior theoretical capacity, swift charge transport, and elevated material utilization [27–30]. Similarly, electrodes modified with metal oxide nanowires, often designed with porous or hollow structures, are gaining traction in LIBs to accommodate substantial volume variation and enhance ion diffusion efficiently [31–35]. $LiCoO_2$, $LiMn_2O_4$, and vanadium oxide nanowires stand out for cathode modification owing to their optimized performance [36–40]. Beyond energy storage, nanowire-modified electrodes find significant applications in electrocatalysis because the structure of nanowires aids in mitigating issues such as dissolution, Ostwald ripening, and aggregation, simultaneously boosting atom utilization during electrocatalysis [41, 42]. Copper nanowires, for instance, are employed for CO_2 reduction [17, 43–46], while platinum group nanowires excel in catalyzing the oxidation of methanol or formic acid [47–53]. Extensive research has been conducted on leveraging nanowire-modified electrodes for other electrocatalytic processes, including oxygen reduction reaction (ORR) [54–56], oxygen evolution reaction (OER) [15, 57–59], hydrogen evolution reaction (HER) [60–63], and overall water splitting [64–66]. More recently, some groups have harnessed the "lightning-rod effect" exhibited by nanowires under an electric field to significantly lower the voltage required for cell electroporation [20, 67–70]. Innovations include the development

Address correspondence to Nian Liu, nian.liu@chbe.gatech.edu; Xing Xie, xing.xie@ce.gatech.edu

of copper-based nanowires (e.g., CuONWs, Cu_3PNWs, Cu_7S_4NWs) and silver nanowires (AgNWs) to modify various substrates, such as copper mesh/foam, graphite felt, and carbon cloth, achieving remarkable inactivation efficiency through irreversible electroporation [70–75].

Nanowires utilized for electrode modification are broadly categorized into two distinct types: anchored and free-standing nanowires. Anchored nanowires are directly synthesized on or etched from the electrode surface, whereas free-standing nanowires are distributed or suspended above the electrode surface. Numerous comprehensive reviews have delineated the application of nanowire-modified electrodes across various domains without differentiating between these two nanowire types [10, 11, 26, 41, 42, 76]. Nonetheless, the characteristics and functionalities of nanowires significantly diverge based on their attachment to the electrode. Anchored nanowires offer enhanced control over their orientation and density, which in turn boosts reproducibility and performance efficiency. This configuration also facilitates superior electron transfer kinetics due to their direct integration with the electrode surface [65, 77]. Conversely, free-standing nanowires, while providing greater surface area exposure for analyte interactions, necessitate an additional binder or structural support to remain affixed to the electrode [78–80]. There exists a wide array of methods for fabricating free-standing nanowires, given their independence from the substrate, rendering them more prevalent compared to their anchored counterparts. Despite the abundance of research and review articles on nanowire-modified electrodes, a comprehensive review of electrodes with anchored nanowires remains absent. Notable, free-standing nanowires can also be affixed to substrates using techniques such as spin-coating [81], freezing drying [75], or ultraviolet (UV) adhesion [82]. However, the bond between free-standing nanowires and the substrate is generally less robust compared to that observed with anchored nanowires, which is beyond the scope of this review.

In this paper, we conducted a comprehensive review of recent advancements in electrodes with anchored nanowires, with a primary focus on energy storage, electrocatalysis, and electric field treatment (EFT). Figure 1 delineates the overarching structure of this review. We systematically categorized various electrodes with anchored nanowires based on their synthesis methodologies, alongside a concise overview of examples for each approach (Table 1). Subsequently, we delved into the modifications made to these electrodes with anchored nanowires, encompassing chemical conversions, functional coatings, and the integration with quantum dots (QDs) or nanoparticles (NPs). Finally, we evaluated different synthesis and modification strategies, offering valuable perspectives on the fabrication of anchored nanowires (Tables 2 and 3).

2 Synthesis of anchored nanowires

There are a variety of bottom-up methodologies employed for the synthesis of anchored nanowires, which can operate within either vapor-phase or solution-phase environments. The prevalent techniques encompass thermal oxidation, vapor–liquid–solid (VLS) growth, solvothermal growth, and chemical precipitation, with materials such as copper, silicon, cobalt, and titanium frequently incorporated into these nanowires. In addition, electrochemical methods, such as electrodeposition and electrochemical anodizing (EC anodizing), are utilized to synthesize anchored nanowires from conductive materials, including metals, semiconductors, and conductive polymers. In contrast, metal-assisted chemical etching (MACE) offers a top-down approach for crafting semiconductor nanowires on homogeneous substrates. An in-depth overview of each synthesis approach, along with illustrative examples, will be elucidated in the subsequent sections.

2.1 Thermal oxidation

A classical method of thermal oxidation involves the growth of CuO nanowires (CuONWs) by calcining a copper substrate in air at temperatures ranging from 400 to 700 °C (Fig. 2(a)) [83]. Although this process was initially considered a vapor-solid (VS)

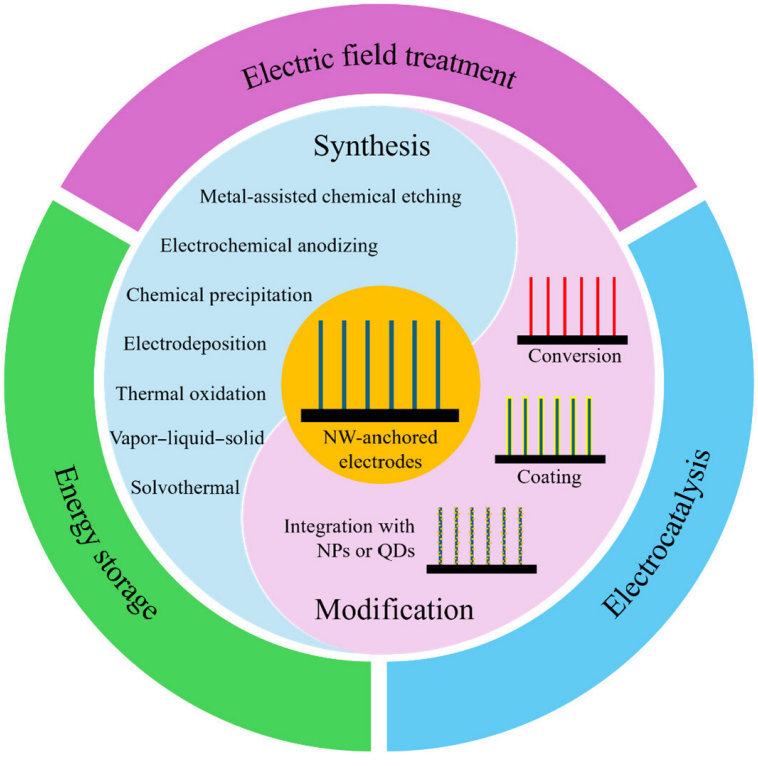

Figure 1 The schematic illustration of the scope of this review, that is, synthesis and modification of anchored nanowires for energy storage, electrocatalysis, and electric field treatment.

Table 1 Summary of recently developed electrodes with anchored nanowires

Nanowires	Substrate	Synthesis/modification	Application	Reference
CuONW	Cu mesh/foam	Thermal oxidation	Drinking water EFT[a]	[71, 72]
PDA[b]-CuONW	Cu foam/wire	Thermal oxidation + coating	Drinking water EFT	[94, 95]
Ni–Co-ZIF[c]@CuONW	Cu mesh	Thermal oxidation + coating	Supercapacitor	[97]
$NiZn_x$@CuONW	Brass mesh	Thermal oxidation + coating	Methanol oxidation	[98]
ZnNiCo-LDH[d]@CuONW	Cu foam	Thermal oxidation + coating	Supercapacitor	[24]
CuNW	Cu mesh	Thermal oxidation + EC[e]/H_2 reduction	CO_2 reduction	[44–46]
IONW[f]	Iron mesh	Thermal oxidation	Bioaerosol EFT	[100]
InP, GaP, GaAs NW	Zn wafer	Vapor–liquid–solid	Solar cell	[104]
SiNW	Stainless-steel foil	Vapor–liquid–solid	LIB[g]	[28, 106]
In_2O_3NW	Si wafer	Vapor–liquid–solid	Supercapacitor	[105, 107]
SiNW	Carbon cloth	Vapor–liquid–solid	LIB	[108]
BNW	Si wafer	Vapor–liquid–solid	Supercapacitor	[110]
Co_3O_4NW	Graphite felt	Solvothermal + annealing	Drinking water EFT	[115–117]
$CoTe_2$NW	Ti foam	Solvothermal + ion exchange	OER[h]	[57]
CoPNW	Graphite felt	Solvothermal + ion exchange	HER[i]	[60]
PPy[j]@Co_3S_4NW	Ni foam	Solvothermal + ion exchange + coating	Energy storage	[22]
CuCoNi oxide NW	Ni foam	Solvothermal + annealing	Pollutant degradation	[118]
POM[k]-ZnCoS NW	Ni foam	Solvothermal + ion exchange + NP[l] integration	Water splitting	[65]
$NiMoO_4$@$NiCo_2O_4$ NW	Ni foam	Solvothermal + annealing + coating	Supercapacitor	[119]
$NiCo_2O_4$ NW	Ni foam	Solvothermal + annealing	LIB	[120]
FeOOH-$NiCo_2S$ NW	Carbon cloth	Solvothermal + ion exchange + NP integration	OER	[59]
Mo-Fe-Ni-P NW	Carbon cloth	Solvothermal + ion exchange	HER	[121]
Fe-TiO_xLNW	Ti foam	Solvothermal + ion exchange + annealing	OER	[15]
$Ni(OH)_2$@$K_2Ti_4O_9$ NW	Ti foam	Solvothermal + ion exchange + coating	Supercapacitor	[122]
MoO_3@TiO_2NW	Carbon cloth	Solvothermal + annealing + coating	LIB	[123]
Reduced TiO_xNW	Graphite felt	Solvothermal + annealing + H_2 reduction	Drinking water EFT	[124, 125]
PbS QD[m]-ZnONW	FTO[n] glass	Solvothermal + QD integration	Solar cell	[126]
NiO@ZnONW	Ni foam	Solvothermal + coating	Supercapacitor	[25]
AgNP-ZnONW	Carbon cloth	Solvothermal + NP integration	Drinking water EFT	[68]
RhNW	Graphite plate	Electrodeposition	HER	[63]
$Li_{0.04}V_2O_5$ NW	Ti foil	Electrodeposition	LIB	[40]
SiNW	Carbon cloth	Electrodeposition	LIB	[133]
PPyNW	Graphite felt	Electrodeposition	Drinking water EFT	[69]
Graphite dendrite	Graphite foam	Electrodeposition + chemical conversion	Supercapacitor & EFT	[134, 135]
PdPtAu, PdPt NW	Glassy carbon	Electrodeposition	Ethanol/methanol oxidation	[136, 137]
(PDA-coated) Cu_3PNW	Cu foam	EC anodizing + ion exchange	Drinking water EFT	[142, 143]
Si/C@CuNW	Cu foil	EC anodizing + H_2 reduction + coating	LIB	[144]
Cu-HHTP[o] NW	Cu mesh	Chemical precipitation + chemical conversion	Drinking water EFT	[148]
CuNW (Cu_2Sb-decorated)	Cu foil	Chemical precipitation + annealing + EC reduction (+ NP integration)	CO_2 reduction	[17, 43]
Ru-CuNW	Cu foam	Chemical precipitation + ion exchange + annealing + EC reduction	Nitrate reduction	[16]
CoNi LDH@CuONW	Cu foam	Chemical precipitation + (annealing) + coating	Supercapacitor	[149]
NiCo-OH@CuONW	Cu foam	Chemical precipitation + (annealing) + coating	Ni-Zn battery	[174]
Cu_xONW	Cu foil	Chemical precipitation + annealing	OER	[58]
AgNP-CuONW	Cu foam	Chemical precipitation + annealing + NP integration	Drinking water EFT	[151]
C@AgNP-Cu_2ONW	Cu foam	Chemical precipitation + annealing + NP integration + coating	Drinking water EFT	[73]
NC[p]@AgNP-Cu_7S_4NW	Cu foam	Chemical precipitation + ion exchange + NP integration + coating	Drinking water EFT	[70]
ZnONW	Zn foil	Chemical precipitation	CO_2 reduction	[154]
SiNW	Si wafer	MACE[q] + QD integration	Solar cell	[165]
SiNW	Si wafer	MACE	LIB	[163]

[a] Electric field treatment; [b] polydopamine; [c] zeolitic imidazolate framework; [d] layered double hydroxide; [e] electrochemical; [f] iron oxide nanowires; [g] lithium-ion battery; [h] oxygen evolution reaction; [i] hydrogen evolution reaction; [j] polypyrrole; [k] polyoxometalates; [l] nanoparticle; [m] quantum dot; [n] fluorine-doped tin oxide; [o] hexahydroxytriphenylene; [p] nitrogen-doped carbon; [q] metal-assisted chemical etching

Table 2 Comparison of different synthesis approaches of anchored nanowires on electrodes

Approach	Materials	Typical process	Advantages	Disadvantages
Thermal oxidation	Metal oxide	The substrate is directly calcinated at a high temperature (e.g., > 400 °C) in air.	1. Simplicity and accessibility 2. High purity of NWs 3. Good control over crystallinity	1. Limited to oxide NWs 2. Mechanisms still unclear 3. High energy consumption
Vapor–liquid–solid growth	Semiconductors and their compounds	The substrate is deposited by catalyst droplets, followed by calcinated at a high temperature in the vapor containing precursors.	1. High control over size, density, and orientation 2. Suitable for complex structures	1. Complexity in catalyst deposition and vapor control 2. Catalyst contamination 3. High energy consumption
Solvothermal growth	Transition metal-based materials	The substrate is immersed in a mixed solution containing solvent, precursor, and reductant, followed by autoclaved at a moderate temperature (e.g., 100 to 300 °C).	1. Relatively low temperature 2. Suitable to synthesize a wide range of NWs 3. Uniformly distributed NWs	1. Long operation time 2. Impurities from the solution 3. Complex chemistry and chemical waste
Electrodeposition	Metals and conductive polymers	The substrate serves as the cathode in an electrolyte containing the precursors and reductants, applied with a negative potential/current.	1. Ambient conditions 2. High precision and control 3. Compatible with industrial large-scale fabrication	1. Limited to conductive NWs 2. Undesired deposition and surface roughness 3. Complex chemistry and electrolyte waste
Electrochemical anodizing	Metal oxide or hydroxide	The substrate serves as the anode in an alkaline condition, applied with a positive potential/current.	1. Good control over dimensions 2. Compatible with industrial large-scale fabrication 3. Environmental friendliness	1. Limited to specific NWs 2. Metastability of NWs 3. Non-uniform distribution of nanowires
Chemical precipitation	Metal hydroxide	The substrate is treated with $(NH_4)_2S_2O_8$ in an alkaline solution under ambient conditions.	1. Simplicity and low cost 2. Uniform distribution of NWs	1. Limited to hydroxide NWs 2. Metastability of NWs 3. Chemical waste
Metal-assisted chemical etching	Semiconductors and their compounds	The substrate is deposited by a noble metal, followed by treated with acid and oxidizing agents under ambient conditions.	1. Simplicity and low cost 2. Vertically aligned NWs with high aspect ratios 3. Suitable for large substrates	1. Limited to semiconductors 2. Undesired etching and surface roughness 3. Etchant waste

Table 3 Summary of different modification approaches of anchored nanowires on electrodes

Modification	Typical process	Purpose
Reduction	Thermal: calcinate the sample in Ar-H_2 mixture (5% H_2) at 300–400 °C Electrochemical: set the sample as cathode, applied with a negative potential/current	1. More active sites due to the absence of oxygen atoms 2. Higher electrical conductivity 3. Resistance to reduction and dissolution
Annealing	Calcinate the sample in air at 300–500 °C for several hours	1. Optimization of the crystalline structure and quality 2. Relaxation and minimization of the strain during nanowire growth 3. Removal of impurities
Ion exchange	Calcinate/autoclave the sample with Na_2S, NaH_2PO_2, Na_2TeO_3 or transition-metal nitrate in an Ar flow/at solvothermal conditions	1. Metalloid properties (e.g., higher electrical conductivity and lower electronegativity) (for phosphorous, sulfur, and tellurium) 2. Intrinsic electrocatalytic properties (for transition metals) 3. Cost-effectiveness and environmental friendliness
Coating/core-shell structure	Various approaches, including sputtering, chemical bath deposition (CBD), atomic layer deposition (ALD), electrodeposition, etc.	1. Mechanical robustness and electrochemical stability (for polydopamine and carbon coating) 2. Porous structures and more redox sites (for metal-organic framework coating) 3. Higher electrical conductivity and electrochemical performance
NP/QD integration	Various approaches, including CBD, spin-coating, dip-coating, etc.	1. More active sites and surface area 2. Higher electrical conductivity (for nanoparticles) 3. Efficient utilization of solar spectrum (for quantum dots)

growth, the underlying mechanism has evolved with extensive investigations into the growth of CuONWs [84]. Various mechanisms encompass VS growth [83, 85], self-catalyzed growth [86], stress-induced diffusion [87, 88], and grain boundary (GB) diffusion [89–91]. The primary distinction between these mechanisms lies in whether the CuONWs originate from vapor deposition or copper ion diffusion. In the VS and self-catalyzed models, CuO vapor is generated from the copper substrate at high temperatures, as described in Eqs. (1) and (2) [83]

$$4Cu + O_2 \rightarrow 2Cu_2O \quad (1)$$

$$2Cu_2O + O_2 \rightarrow 4CuO \quad (2)$$

CuO vapor subsequently migrates and diffuses onto the cooler electrode surface, inducing supersaturation that leads to nucleation and subsequent growth of nanowires, as shown in Fig. 2(b). Notably, in the self-catalyzed model, copper also melts and forms islands on the substrate. These copper islands act as catalysts for CuO vapor deposition, although they will be finally oxidized into CuO as well [86, 92]. Conversely, in the stress-induced and GB diffusion models, a three-layer structure "Cu/Cu_2O/CuO" (Fig. 2(c)) forms through the diffusion of copper ion toward the substrate-oxygen interface, as described in Eqs. (3) and (4) [84]

$$2Cu + O_2 \rightarrow 2CuO \quad (3)$$

$$Cu + CuO \rightarrow Cu_2O \quad (4)$$

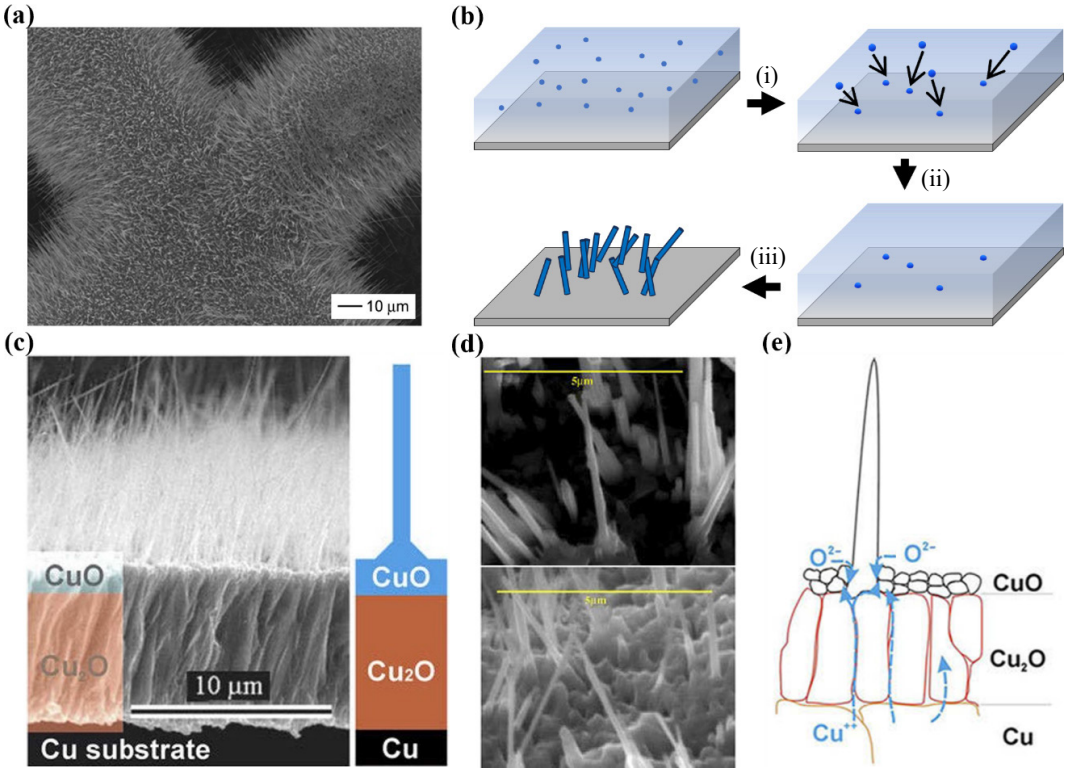

Figure 2 Different mechanisms behind the synthesis of CuONWs via thermal oxidation. (a) SEM image of CuONWs grown at 500 °C for 4 h. Reproduced with permission from Ref. [83], © American Chemical Society 2002. (b) Schematic illustration of VS growth of nanowires: (i) precursor vapor migrates and diffuses onto the cooler substrate surface, (ii) supersaturation causes nucleation of growth species, and (iii) sebsequent growth of anchored nanowires. (c) Cross-sectional view of two oxide layers and CuONWs grown at 400 °C. Reproduced with permission from Ref. [84], © The Materials Research Society 2018. (d) SEM images of CuONWs grown at 675 °C for 15 min, revealing growth of nanowires from larger crystallites. Reproduced with permission from Ref. [88], © Elsevier B.V 2005. (e) Schematic illustration of the GB diffusion of Cu ions in the substrate. Reproduced with permission from Ref. [89], © AIP Publishing 2009.

For the stress-induced model, the diffusion of copper ions results in the formation of small CuO crystallites to relieve stress, from which the nanowires begin to grow (Fig. 2(d)) [88]. For the GB model, ion diffusion along the grain boundaries occurs more rapidly, leading to the nucleation and subsequent growth of CuONWs (Fig. 2(e)) [89]. Additionally, the influence of the oxygen concentration gradient has been explored within the GB model to elucidate the specific temperature ranges conducive to CuONW growth [90]. So far, the GB model, which considers the oxygen concentration gradient, has been more widely accepted because it addresses several limitations of other models [84]. For instance, both the VS and self-catalyzed models fail to explain why the growth temperature of CuONWs (400–700 °C) is significantly lower than the melting points of Cu, Cu_2O, and CuO (1085, 1243, and 1326 °C, respectively) [88]. The stress-induced model does not account for the suppression of CuONW growth at temperatures exceeding 700 °C [84], while the initial GB model overlooks the influence of the gaseous environment on nanowire growth, such as the observed slower growth rates of CuONWs under higher oxygen flow rates [93].

Despite the divergent and controversial mechanisms reported in the literature, the growth process of CuONWs via thermal oxidation has attracted increasing attention due to its simplicity and accessibility. Xie group calcinated various copper substrates (i.e., foam, mesh, wire) at 400 °C for 2 h to obtain CuONWs, subsequently enveloping these nanowires with a polydopamine (PDA) layer for elevated mechanical strength (Fig. 3(a)) [72, 94, 95]. Hussain et al. processed copper mesh at 500 °C for 4 h and modified CuONWs with the metal-organic framework (MOF)-derived materials, showcasing the potential for energy storage applications (Fig. 3(b)) [96, 97]. Similarly, Poudel et al. treated copper foam at 500 °C for 4 h and coated CuONWs with ZnNiCo-LDH, a MOF-derived material, to develop a supercapacitor with elevated energy density [24]. Han et al. explored the calcination of brass mesh under diverse conditions (i.e., temperature and duration), depositing a NiZn alloy film on CuONWs for electrocatalytic oxidation of methanol (MOR) (Fig. 3(c)) [98]. We can find from these examples that with the advancements in material science, functional coatings to refine the pre-formed nanowires are gaining momentum. Moreover, many studies leveraged thermal and electrochemical reduction to convert CuONWs into copper nanowires (CuNWs) for electrocatalytic reduction of CO_2 (Fig. 3(d)) [44–46]. These further modifications are pivotal for achieving superior electrocatalytic or electrochemical performance, a topic that will be elaborated upon in Section 3.

In addition to CuONWs, the synthesis of other metal oxide nanowires is straightforward through thermal oxidation [99]. For example, Wang et al. demonstrated the growth of iron oxide nanowires (IONWs) by calcinating pure iron mesh at 700 °C for 6 h [100]. Similarly, Dlugosch et al. substituted pure iron mesh with a low-carbon steel sheet, successfully fabricating IONWs on the substrate [101]. Some groups also employed thermal oxidation to fabricate free-standing oxide nanowires, such as ZnO, Ga_2O_3, MgO, and SnO_2 nanowires by calcinating corresponding metal powders, which is beyond the scope of this review [92, 102, 103]. In general, thermal oxidation is capable of producing high-purity anchored nanowires with good control over crystallinity but suffers from the limitations of oxide nanowires and high energy consumption.

2.2 Vapor–liquid–solid growth

Vapor–liquid–solid growth is a kind of spontaneous growth, driven by the reduction of Gibbs free energy through phase transformation [2]. Liquid phase materials, such as impurities or catalysts, play a pivotal role in guiding and confining the nanowire

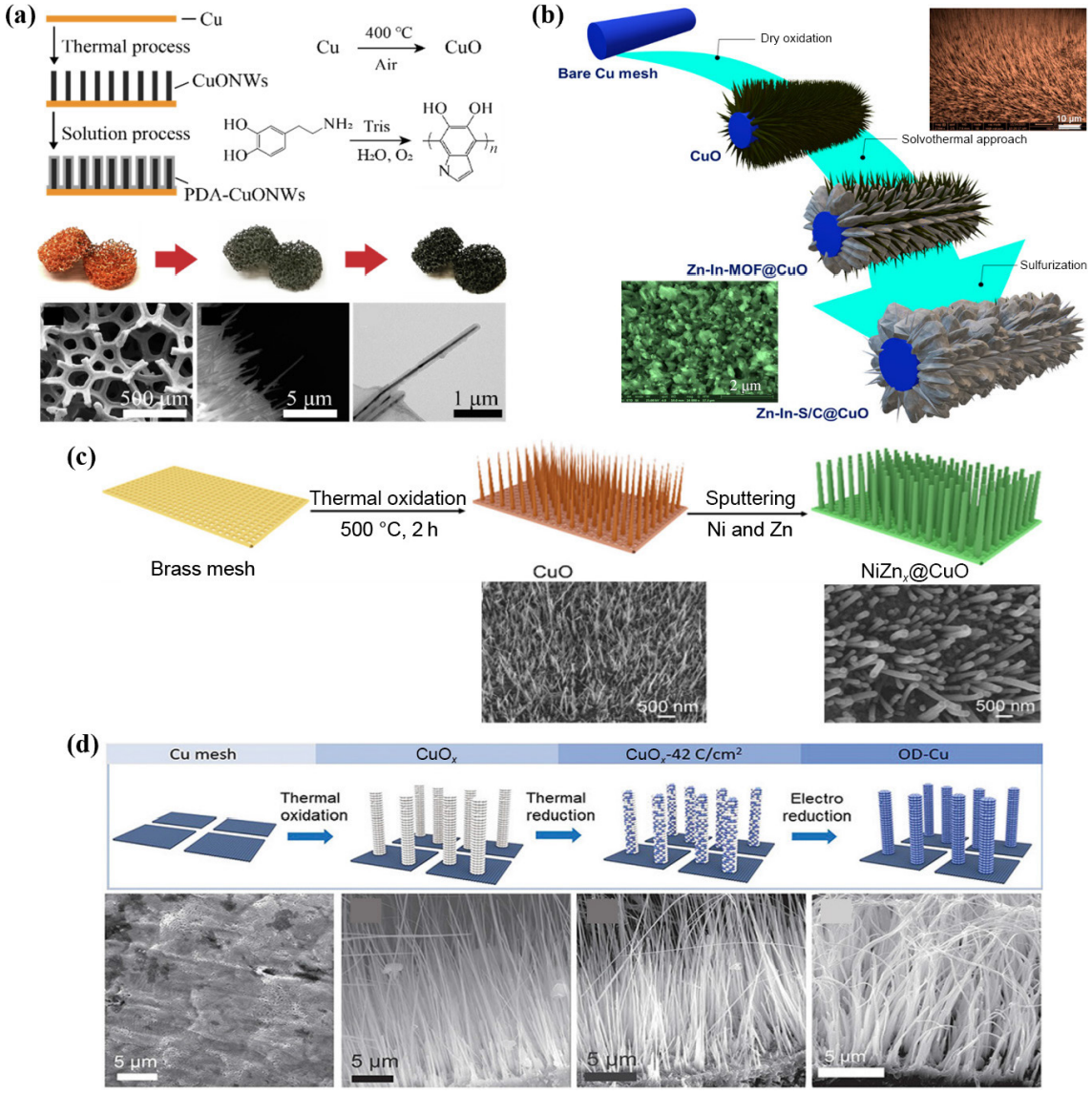

Figure 3 Examples of copper-based nanowires synthesized via thermal oxidation. (a) Schematic illustration of the synthesis of PDA-coated CuONWs, and corresponding optical and SEM images for each step (from left to right). Reproduced with permission from Ref. [94], © Elsevier B.V 2019. (b) Schematic illustration of the synthesis of Zn-In-S/C@CuONWs, and corresponding SEM images for the second and third steps. Reproduced with permission from Ref. [96], © American Chemical Society 2023. (c) Schematic illustration of the synthesis of $NiZn_x$@CuONWs, and corresponding SEM images for each step. Reproduced with permission from Ref. [98], © American Chemical Society 2023. (d) Schematic illustration of the synthesis of CuNWs, and corresponding SEM images for each step. Reproduced with permission from Ref. [46], © American Chemical Society 2020.

growth [2]. In a typical VLS process, the catalyst droplets are formed through techniques such as lithography [104], evaporation [28], and sputtering [105], followed by the introduction of the vapor containing growth species. These species exhibit a preference for depositing on the liquid surface of catalyst droplets, attributed to a higher accommodation coefficient compared to the substrate surface [2]. A higher accommodation coefficient represents that a greater fraction of impinging vapor molecules become accommodated on the substrate, resulting in a higher condensation rate (e.g., atoms·cm^{-2}·s^{-1}). Subsequently, the growth species diffuse toward and precipitate at the substrate-liquid interface. Continuous precipitation of growth species thus separates the substrate and the liquid droplet, leading to nanowire elongation, as shown in Fig. 4(a).

Gold is frequently employed as a catalyst in VLS processes. For example, Otnes et al. utilized nanoimprint lithography (NIL) to pattern gold catalysts on a zinc wafer, facilitating the growth of InP nanowires at 550 °C in a vapor mix comprising PH_3, trimethylindium (TMIn), diethylzinc (DEZn), and HCl, with H_2 serving as the carrier gas (Fig. 4(b)) [104]. Alternative materials like GaP and GaAs nanowires were also accessible by replacing TMIn and PH_3 with TMGa and AsH_3, respectively [104]. E-beam evaporation was utilized to deposit gold catalysts for the growth of silicon nanowires (SiNWs) on stainless-steel foils using SiH_4/H_2 as a precursor [28, 106]. Furthermore, Tuzluca et al. sputtered gold catalysts on a silicon wafer for the growth of In_2O_3 nanowires (In_2O_3NWs) by calcinating the substrate and indium powder in a tube furnace at different temperature zones ranging from 600 to 1000 °C (Fig. 4(c)) [105, 107].

Beyond gold catalysts, Storan et al. thermally evaporated tin catalysts onto the carbon cloth and grew SiNWs using phenylsilane as a precursor (Fig. 4(d)) [108]. Collins et al. also used tin as the catalyst to decorate pre-formed $Cu_{15}Si_4$ nanowires with SiNWs at 460 °C, which could increase the capacity of LIBs [109]. Furthermore, iron oxide has served as a catalyst for boron nanowire (BNW) synthesis, involving calcination of a silicon wafer with boron and boron trioxide at high temperatures (i.e., 1200 °C) in an argon and hydrogen gas flow (Fig. 4(e)) [110]. Notably, the VLS method offers controlled manipulation over the diameter and density of the grown nanowires, depending on the

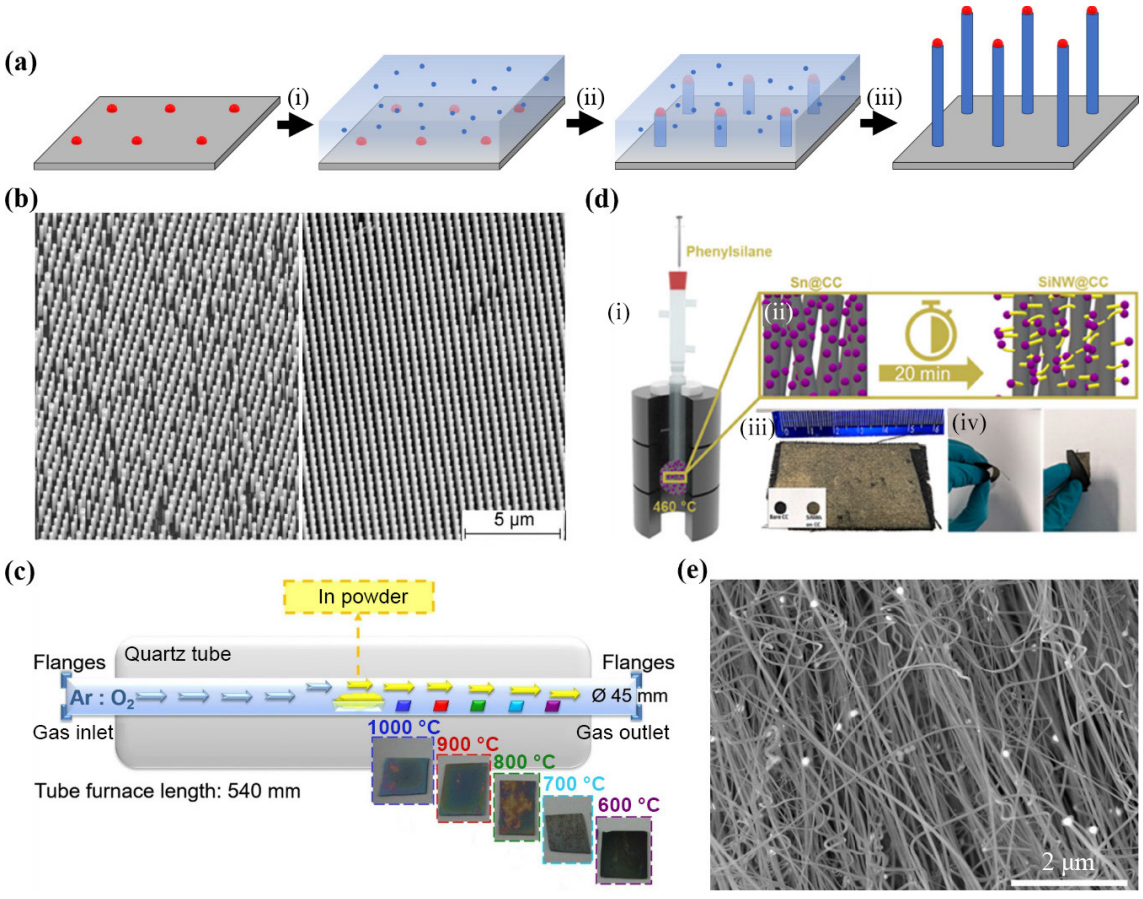

Figure 4 VLS growth. (a) Schematic illustration of VLS growth of nanowires: (i) growth species preferentially deposit on the liquid surface, (ii) growth species diffuse toward and precipitate at the substrate-liquid interface, and (iii) continuous precipitation leads to nanowire elongation. (b) SEM images of InPNWs grown from NIL-defined gold seed particle arrays without (left) and with (right) heating pretreatment. Reproduced with permission from Ref. [104], © Tsinghua University Press and Springer-Verlag Berlin Heidelberg 2016. (c) Schematic illustration of the setup for In_2O_3NW synthesis. Reproduced with permission from Ref. [105], © Elsevier B.V. 2017. (d) Schematic illustration of the (i) setup and (ii) SiNW growth on carbon cloth (CC), (iii) optical image of SiNW coverage on CC with bare CC and SiNW@CC inserted, and (iv) images showing the flexible nature of SiNW@CC. Reproduced from Ref. [108], © Storan, D. et al. 2022. (e) FESEM image of BNWs from top view. Reproduced with permission from Ref. [110], © Elsevier B.V. 2019.

size and distribution of catalyst droplets, which surpasses the VS method [2]. In addition, the VLS method has found extensive application in the synthesis of III-V compound nanowires (e.g., InP, InAs, GaAs) for optoelectronic devices and sensors [111–114], but falls outside the scope of this review.

2.3 Solvothermal growth

Solvothermal growth is also a kind of spontaneous growth, where the reduction of Gibbs free energy is facilitated by chemical reactions [2]. A typical solvothermal growth involves dissolving precursors, reactants, and structure-directing agents in a solvent, followed by immersing the substrate into this mixture. The mixture is subsequently autoclaved at elevated temperatures and pressures to promote nanowire growth, as illustrated in Fig. 5(a) [1]. Due to its high compatibility with various substrates and growth species, solvothermal growth has become a prevalent technique for synthesizing electrodes with anchored nanowires [1]. A classic solvothermal recipe for the synthesis of cobalt-based nanowires is composed of $Co(NO_3)_2$, NH_4F, and urea. Liu group demonstrated this by immersing graphite felt in a solution derived from these ingredients and autoclaving at 120 °C for 10 h, resulting in the formation of $Co(OH)_2$ nanowires. These were then dehydrated to Co_3O_4 nanowires (Co_3O_4NWs) by annealing the graphite felt with anchored nanowires at 400 °C, as illustrated in Fig. 5(b) [115–117]. Similarly, Ji et al. subjected the same mixture to autoclaving at 100 °C for 8 h, followed by a secondary solvothermal process with Na_2TeO_3 and N_2H_4 to yield $CoTe_2$ nanowires on titanium foam for electrocatalytic OER [57]. Interestingly, the variance in the initial solvothermal products—$Co(OH)_2$ versus Co(OH)F nanowires—reported by Liu group and Ji et al., respectively, underscored the influence of concentration, ratios, and autoclaving conditions. Furthermore, employing the same initial mixture (without identifying the intermediate nanowires), Ren et al. obtained CoP nanowires (CoPNWs) by calcinating at 300 °C in the presence of NaH_2PO_2 in an argon atmosphere, a process referred to as phosphating [60]. Huo et al. modified the recipe slightly to produce Co_3O_4 nanowires on nickel foam, which were then transformed into Co_3S_4 nanowires (Co_3S_4NWs) through a solvothermal sulphuration process involving Na_2S ion exchange, followed by coating with polypyrrole (Fig. 5(c)) [22].

Other metals have also been explored to integrate into cobalt-based nanowires. Wang et al. incorporated $Cu(NO_3)_2$ to synthesize CuCoNi oxide nanowires for the electrocatalytic degradation of bisphenol A [118]. Similarly, Gautam et al. introduced $Zn(NO_3)_2$, followed by solvothermal sulphuration and coating with polyoxometalates (POM), to fabricate POM@ZnCoS nanowires for overall water splitting [65]. By adding $Ni(NO_3)_2$ to the solvothermal mixture, Zhao et al. and Zhou et al. developed nickel foams with anchored $NiCo_2O_4$ nanowires for supercapacitors and lithium-ion batteries (LIBs), respectively [119, 120]. Additionally, Li et al. enhanced the Ni-Co mixture with $FeSO_4$ to obtain NiCo-OH/FeOOH nanowires on carbon cloth, which were subsequently converted to FeOOH-integrated $NiCo_2S_4$ nanowires through an ion exchange process with Na_2S (Fig. 5(d)) [59]. Moreover, Zhao et al. prepared Mo-Fe-Ni-P nanowires by immersing carbon cloth

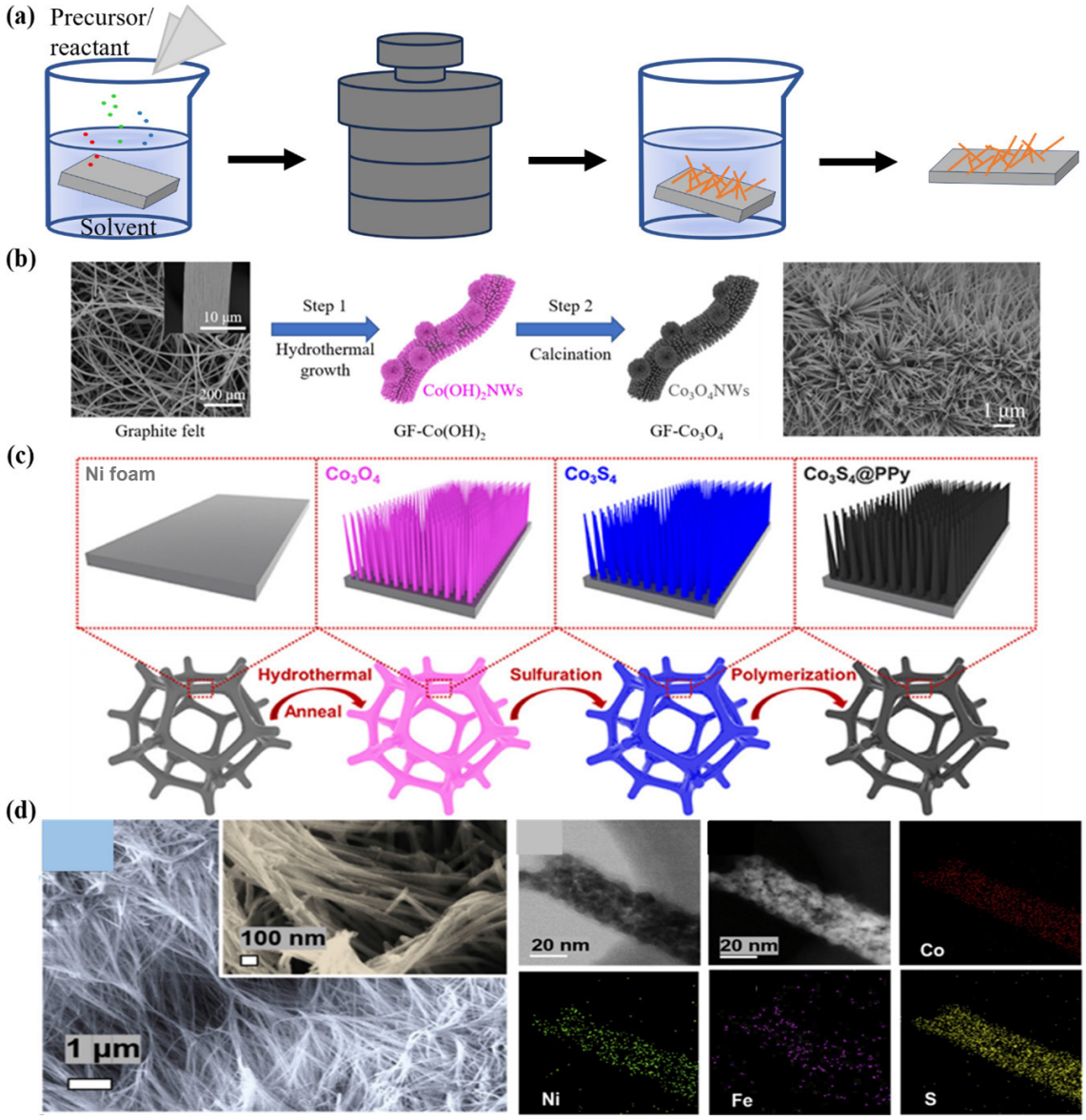

Figure 5 Cobalt-based nanowires synthesized via solvothermal growth. (a) Schematic illustration of solvothermal growth of nanowires. (b) Schematic illustration of the synthesis of Co_3O_4NWs, and SEM image of Co_3O_4NWs. Reproduced with permission from Ref. [115], © Elsevier B.V. 2022. (c) Schematic illustration of the synthesis of PPy@Co_3S_4NWs. Reproduced with permission from Ref. [22], © Elsevier Ltd. 2020. (d) SEM images of FeOOH-$NiCo_2S_4$ nanowires with an enlarged image inserted (left), and STEM images of FeOOH-$NiCo_2S_4$ nanowires and corresponding element mapping pattern (right). Reproduced with permission from Ref. [59], © Elsevier Ltd. 2020.

in a solution of Na_2MoO_4, $Ni(NO_3)_2$, $Fe(NO_3)_3$, NH_4F, and urea, followed by autoclaving and ion exchange with NaH_2PO_4 [121].

Furthermore, titanium-based nanowires have garnered significant attention for their potential in various applications. Zhao et al. demonstrated the synthesis of $K_2Ti_4O_9$ nanowires by immersing titanium foam in a 10 M KOH and heating at 90 °C for 6 h [15]. These nanowires were then subjected to ion exchange using $Fe(NO_3)_3$ and annealing at 450 °C to obtain Fe-TiO_x layered nanowires (Fe-TiO_xLNWs, x represents the degree of ion exchange) [15]. During this process, K^+ and Fe^{3+} ions occupied the TiO_6 octahedra cavities, resulting in FeO_x integration into TiO_2 nanowires (Fig. 6(a)) [15]. In parallel, Zhou et al. employed a $Ni(NO_3)_3$ solution for the ion exchange of the titanium foam with anchored $K_2Ti_4O_9$ nanowires, ultimately achieving $Ni(OH)_2$-coated $K_2Ti_4O_9$ nanowires for supercapacitor applications (Fig. 6(b)) [122]. The modification of these titanate nanowires will be further discussed in Section 3.1. Additionally, the use of titanium butoxide and HCl, in conjunction with $TiCl_4$ and alcohol for seeding, has become a favored approach for the synthesis of titanium-based nanowires. For instance, Liang et al. grew TiO_2 nanowires (TiO_2NWs) by autoclaving a fluorine-doped tin oxide (FTO) glass slide in a mixture of these components at 150 °C for 12 h, followed by hydrogenation and integration with QDs for photoelectrochemical water splitting (Fig. 6(c)) [66]. Wang et al. incorporated acetone into this recipe and autoclaved a Ti-seeded carbon cloth at 200 °C for 2 h to grow TiO_2NWs, followed by MoO_3 coating to increase the capacity and conductivity of the electrode for LIBs (Fig. 6(d)) [123]. Similarly, Liu group adopted this method with minor adjustments to grow TiO_2NWs on graphite felt and reduced them with hydrogen (i.e., reduced TiO_xNWs) for enhanced EFT [124, 125].

In addition to cobalt- and titanium-based nanowires, ZnO nanowires stand out for their broad applications in energy storage domains. Wang et al. prepared a mixed solution of $Zn(NO_3)_2$, NH_3OH, hexamethylenetetramine (HMT), and polyethyleneimine to grow ZnO nanowires (ZnONWs) on a FTO glass slide and integrated with PbS QDs for solar cell (Fig. 6(e)) [126]. Lin et al. also seeded the FTO glass substrate with ZnO film and proceeded with solvothermal growth in a $ZnCl_2$ and HMT mixed solution at 125 °C for 4 h to produce ZnONWs [127]. Similarly, Chebrolu et

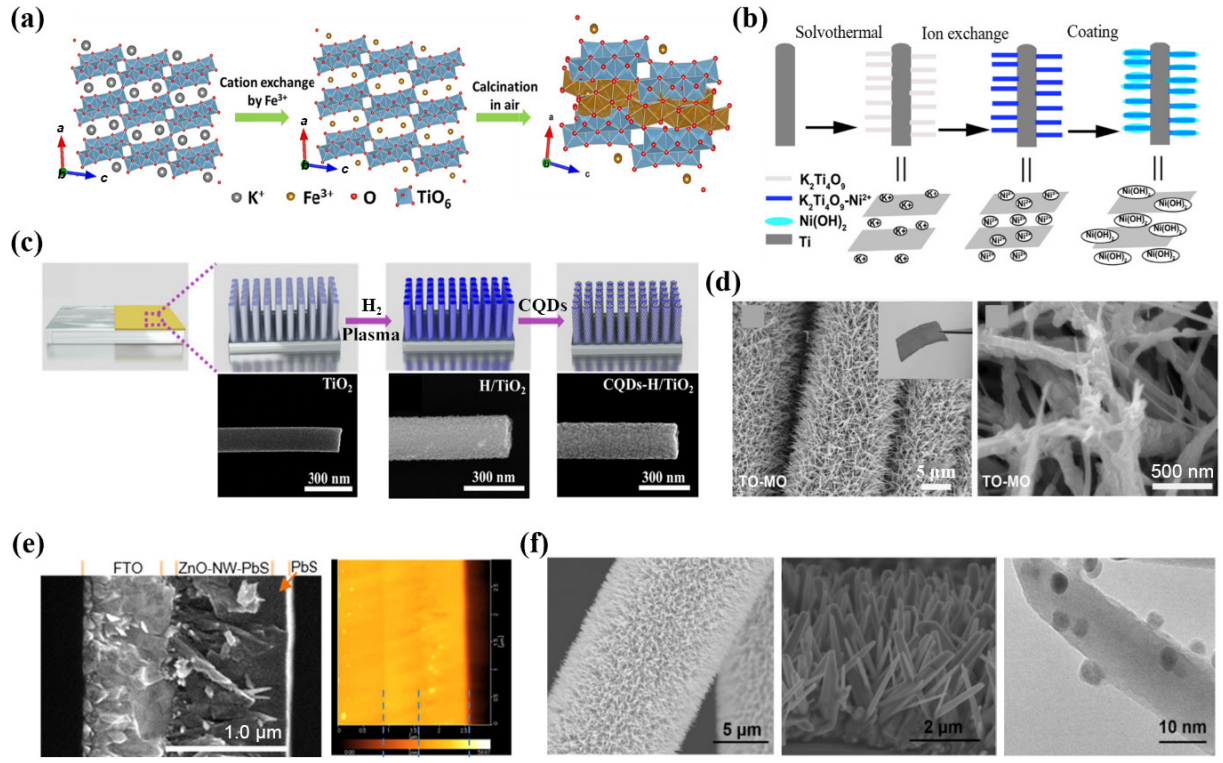

Figure 6 Titanium- and zinc-based nanowires synthesized via solvothermal growth. (a) Schematic illustration of the structures of $K_2Ti_4O_9$ nanowires, $Fe_xTi_4O_9$ nanowires, and Fe-TiO_xLNWs (from left to right). Reproduced with permission from Ref. [15], © Elsevier Ltd. 2017. (b) Schematic illustration of the synthesis of $Ni(OH)_2$@$K_2Ti_4O_9$ nanowires. Reproduced with permission from Ref. [122], © American Chemical Society 2014. (c) Schematic illustration of the synthesis of CQDs-H/TiO_2NWs on FTO glass and corresponding SEM images for each step. Reproduced with permission from Ref. [66], © American Chemical Society 2019. (d) SEM images of MoO_3-coated TiO_2NWs on carbon cloth. Reproduced with permission from Ref. [123], © WILEY-VCH Verlag GmbH & Co. KGaA, Weinheim 2015. (e) Cross-sectional SEM (left) and AFM (right) images of the PbS QD/ZnONW-modified solar cell. Reproduced with permission from Ref. [126], © American Chemical Society 2021. (f) SEM images (left and middle) of ZnONWs on carbon cloth, and TEM image (right) of AgNPs attached to ZnONWs. Reproduced with permission from Ref. [68], © Elsevier Ltd. 2017.

al. used $Zn(NO_3)_2$, HMT, and NH_4F to grow ZnONWs on nickel foam and deposited NiO nanosheets on ZnONW-anchored nickel foam to improve the performance of supercapacitor [25]. Tian et al. seeded carbon cloth with ZnO film and autoclaved it in $Zn(NO_3)_2$ and NH_3OH mixed solution at 95 °C for 75 min to grow ZnONWs, followed by silver nanoparticles (AgNPs) integration (Fig. 6(f)) [68]. A notable observation across these approaches is the diverse range of substrates—ranging from glass slides to nickel foam and carbon cloth—often pre-seeded with a thin film of ZnO or TiO_2 before solvothermal growth of ZnONWs or TiO_2NWs. This contrasts with the procedures for cobalt-based nanowires, highlighting the adaptability of solvothermal techniques to varied materials and applications. In general, despite the straightforward nature of the solvothermal approach, the solution preparation, along with meticulous temperature and time control, can present challenges. Additionally, the multistep processes inherent to this approach add complexity to practical fabrication.

2.4 Electrodeposition

Electrodeposition, also known as electrochemical deposition, is primarily considered a template-based synthesis method [2]. This process involves the migration of charged species, originating either from the counter electrode or the electrolyte, toward the target substrate that serves as the cathode (i.e., working electrode), followed by the reduction of these species on the substrate surface [2]. Therefore, electrodeposition is only applicable to conductive materials, such as metals, semiconductors, and some conductive polymers, which allow the current to pass through the deposited layer to continue the electrodeposition process [2]. For the electrodeposition of nanowires, a porous template is typically required to confine the deposition, leading to the growth of nanowires (Fig. 7(a)). Among various templates, nanoporous anodic alumina oxide (AAO) stands out for its tunable pore dimensions, mechanical strength, and thermal stability [128, 129]. For instance, Schiavi et al. fabricated AAO templates by one-step anodizing in 0.3 M H_2SO_4 solution with a potential of 25 V, and then electrodeposited cobalt nanowires (CoNWs) using $CoSO_4$, $CoCl_2$, and H_3BO_3 as the electrolyte [130]. Zhang et al. employed a solvothermal approach to form a gold nanoparticle film inside commercial AAO templates and then electrodeposited Rh nanowires (RhNWs) using $HClO_4$, $RhCl_3$, and sodium citrate as the electrolyte (Fig. 7(b)) [63]. Guiliani et al. treated high-purity aluminum foil by a two-step anodizing process and electrodeposited Ni and Ni/Au nanowires on various substrates (i.e., silicon wafers, copper tapes/wires) [131]. In a typical electrodeposition process, the AAO templates must be meticulously dissolved using a NaOH solution after the nanowire synthesis to ensure the integrity of the nanowires [63, 131].

In general, since the morphology of electrodeposited nanowires is significantly dependent on the template, the fabrication of AAO is usually of high priority during electrodeposition, which presents considerable challenges and complexities that demand further detailed investigation [128, 130]. For instance, the two-step process is predominantly used to obtain high-quality AAO templates due to the more uniform pore size and distribution of AAO nanotubes than those produced by a single anodizing cycle [132]. Specifically, the two-step process involves two anodizing cycles. The first anodizing step creates a preliminary oxide layer, which is subsequently removed to reveal a patterned aluminum surface. The second anodizing step is then performed on this patterned surface, resulting in a highly ordered AAO template.

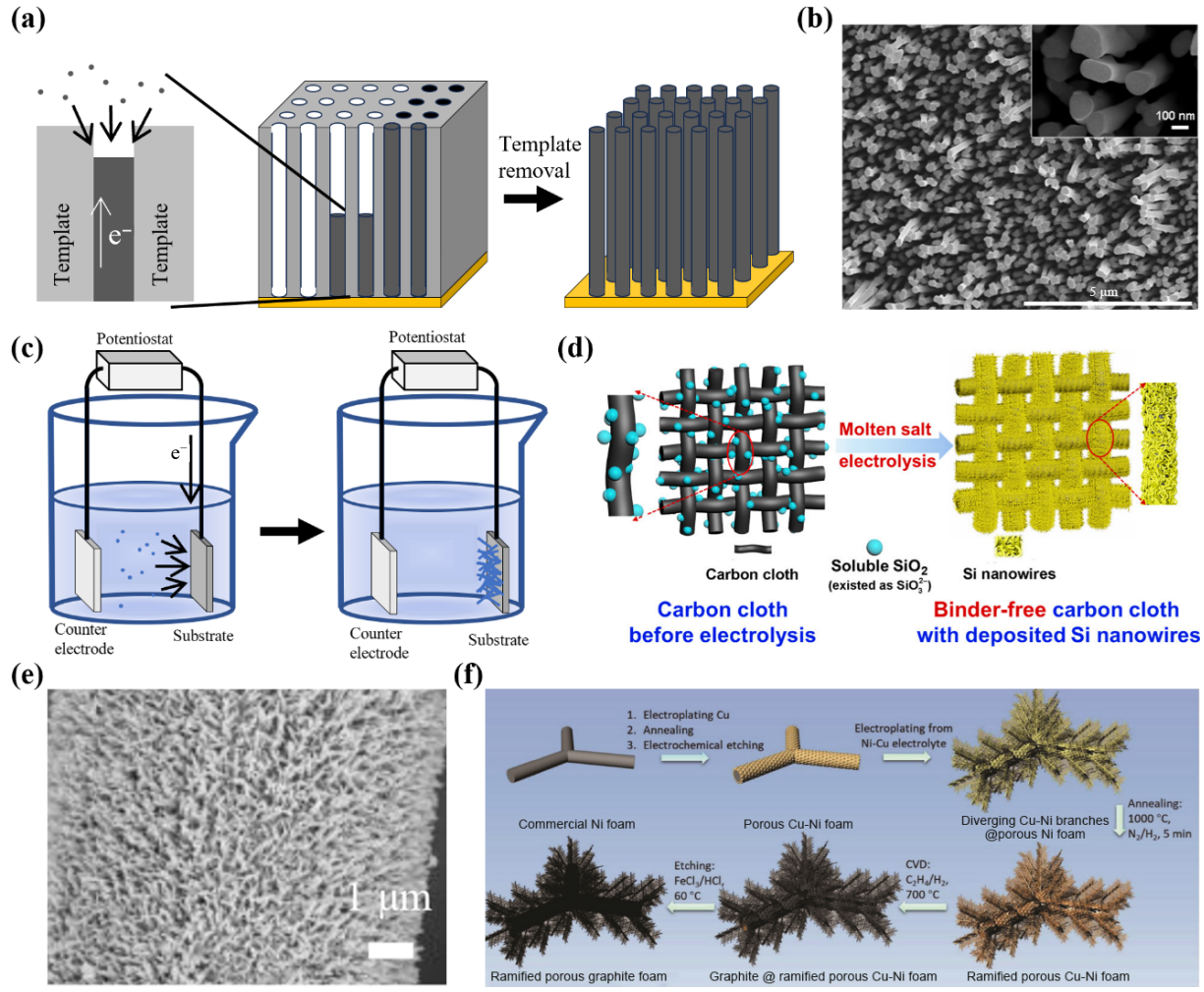

Figure 7 Electrodeposition. (a) Schematic illustration of electrodeposition of nanowires using porous templates. (b) SEM image of RhNWs electrodeposited at −0.3 V in electrolyte containing 1.6 mM $RhCl_3$, 0.1 M $HClO_4$ and 40 mM citrate. Reproduced from Ref. [63], © Zhang, L. Q. et al. 2017. (c) Schematic illustration of electrodeposition of nanowires without templates. (d) Schematic illustration of the carbon cloth before and after electrodeposition of SiNWs. Reproduced with permission from Ref. [133], © American Chemical Society 2019. (e) SEM image of PPyNWs on graphite felt. Reproduced with permission from Ref. [69], © Elsevier Ltd. 2021. (f) Schematic illustration of the synthesis of dendritic graphite foams. Reproduced with permission from Ref. [134], © WILEY-VCH Verlag GmbH & Co. KGaA, Weinheim 2018.

The fabrication process of AAO templates belongs to electrochemical anodizing, a technique capable of synthesizing self-aligned metal oxide nanotubes or nanowires, which will be detailed in the next section. Notably. electrodeposition is rarely utilized for synthesizing anchored nanowires, likely due to the simplicity of directly attaching free-standing nanowires to the substrate rather than employing AAO templates.

Recently, the electrodeposition of nanowires has been explored without using the porous templates, which can be considered as a spontaneous or self-propagating process [2]. The principle is that after the initial deposition of the growth species, the electric field and current density between the nanowire tips (or nanoparticles at the beginning) and the counter electrode are greater than those between the substrate and the counter electrode because of a shorter distance. Hence, the growth species will prefer to deposit on the nanowire tips, resulting in continuous growth of the nanowires (Fig. 7(c)) [2]. Hua et al. used a mixed solution composed of NH_4VO_3, oxalic acid, HMT, and $LiNO_3$ to deposit $Li_{0.04}V_2O_5$ nanowires on Ti foil, followed by annealing at 200–400 °C for high-density LIB [40]. Weng and Xiao used a molten salt containing NaCl, $CaCl_2$, and soluble SiO_2 as the electrolyte to deposit SiNWs on carbon cloth (Fig. 7(d)) [133]. Liu group used a mixed electrolyte composed of phosphate buffer solution, pyrrole monomer, and p-toluenesulfonate and applied a voltage of −2.4 V to deposit polypyrrole nanowires (PPyNWs) on graphite felt (Fig. 7(e)) [69]. Moreover, Li et al. and Luo et al. electrodeposited diverging Ni/Cu branches on a nickel foam and grew graphite dendritic through chemical vapor deposition (CVD) with C_2H_4 [134, 135]. They then removed the metal foam core (*i.e.*, dendritic graphite foams) by selective chemical etching using $FeCl_3$ and HCl, obtaining dendritic graphite foams (DGFs) (Fig. 7(f)) [134, 135]. Furthermore, Tang et al. utilized a square-wave potential (SWP) for the electrodeposition of alloy nanowires, such as PdPtAu and PdPt, on glassy carbon electrodes (GCE) [136, 137]. Interestingly, these nanowires exhibit a helical structure, resulting in enhanced electrocatalytic oxidation performance [136]. Generally, compared to vapor-based or solvothermal growth, electrodeposition necessitates control over a broader range of parameters, including potential, current, and electrolyte. Therefore, fewer studies directly apply electrochemical approaches to synthesize anchored nanowires, but electrodeposition is a commonly used approach for coating, which will be discussed in Section 3.2.

2.5 Electrochemical anodizing

Anodizing is another electrochemical technique capable of synthesizing self-aligned metal oxide arrays, which has a distinct setup and principle from electrodeposition. In a typical EC

anodizing process, the substrate (e.g., metal foil) serves as the anode, subjected to a positive potential or current, while inert materials such as platinum and graphite serve as the cathode. The metal is subsequently oxidized to its ion form, as described in Eq. (5), where M represents the substrate metal and n represents the valence of the metal.

$$M \rightarrow M^{n+} + ne^{-} \quad (5)$$

The mechanism behind EC anodizing can be delineated by the following steps: (1) the M^{n+} ions are solvated in the electrolyte, resulting in continuous dissolution of the metal (i.e., electropolishing), (2) the M^{n+} ions react with O^{2-} or OH^{-} (dependent on the electrolyte) to form a compact oxide/hydroxide layer, (3) under a well-controlled condition, competition between solvatization and oxide/hydroxide formation leads to the growth of self-ordered metal oxide/hydroxide (i.e., nanotubes or nanowires), (4) disorganized rapid growth of oxide nanotube or nanowires, and (5) thick self-organized mesoporous layers form after long-term operation [138, 139]. Figure 8(a) illustrates the process of EC anodizing. As mentioned in Section 2.4, Al_2O_3 nanotube arrays with well-defined periodic orders, fabricated through EC anodizing, find an extensive application as templates for electrodeposition. This fabrication technique has also been thoroughly explored for other materials, including TiO_2 and Fe_2O_3 nanotubes [139–141]. In addition, EC anodizing has been widely employed in the synthesis of anchored nanowires, such as $Cu(OH)_2$ nanowires and ZnONWs.

For instance, Huo et al. processed copper foam in a 1.5 M NaOH solution for 15 min at a constant current density of 12.5 mA/cm^2, resulting in the formation of $Cu(OH)_2$ nanowires [142, 143]. Huo et al. then converted $Cu(OH)_2$ nanowires into Cu_3PNWs and coated a PDA layer on the copper foam with anchored nanowires (Fig. 8(b)) [142, 143]. Similarly, Su et al. subjected copper foil to anodizing in a 1 M KOH solution at a constant voltage of 1.2 V to obtain $Cu(OH)_2$ nanowires, followed by hydrogen reduction at 400 °C and coated with magnetron Si/C shell for LIBs (Fig. 8(c)) [144]. Moreover, Tantray and Shah investigated the effects of electrolyte concentration ($KHCO_3$), potential applied (graphite as the counter electrode), and operation time on the ZnONW morphology (Fig. 8(d)) [145]. In addition, Tello et al. used an organic-based electrolyte consisting of $C_2H_6O_2$, NaOH, and NH_4F for the anodization of zinc foil, discovering that the nanowire morphology under 30 V was superior to those under 20 and 40 V (Fig. 8(e)) [146]. Interestingly, the presence of fluoride ions dissolved the surface of pre-formed ZnONWs, which in turn caused reprecipitation (Eqs. (6)–(9)) [146].

$$Zn(s) + 2OH^{-}(aq) \rightarrow ZnO(s) + 2e^{-} \quad (6)$$

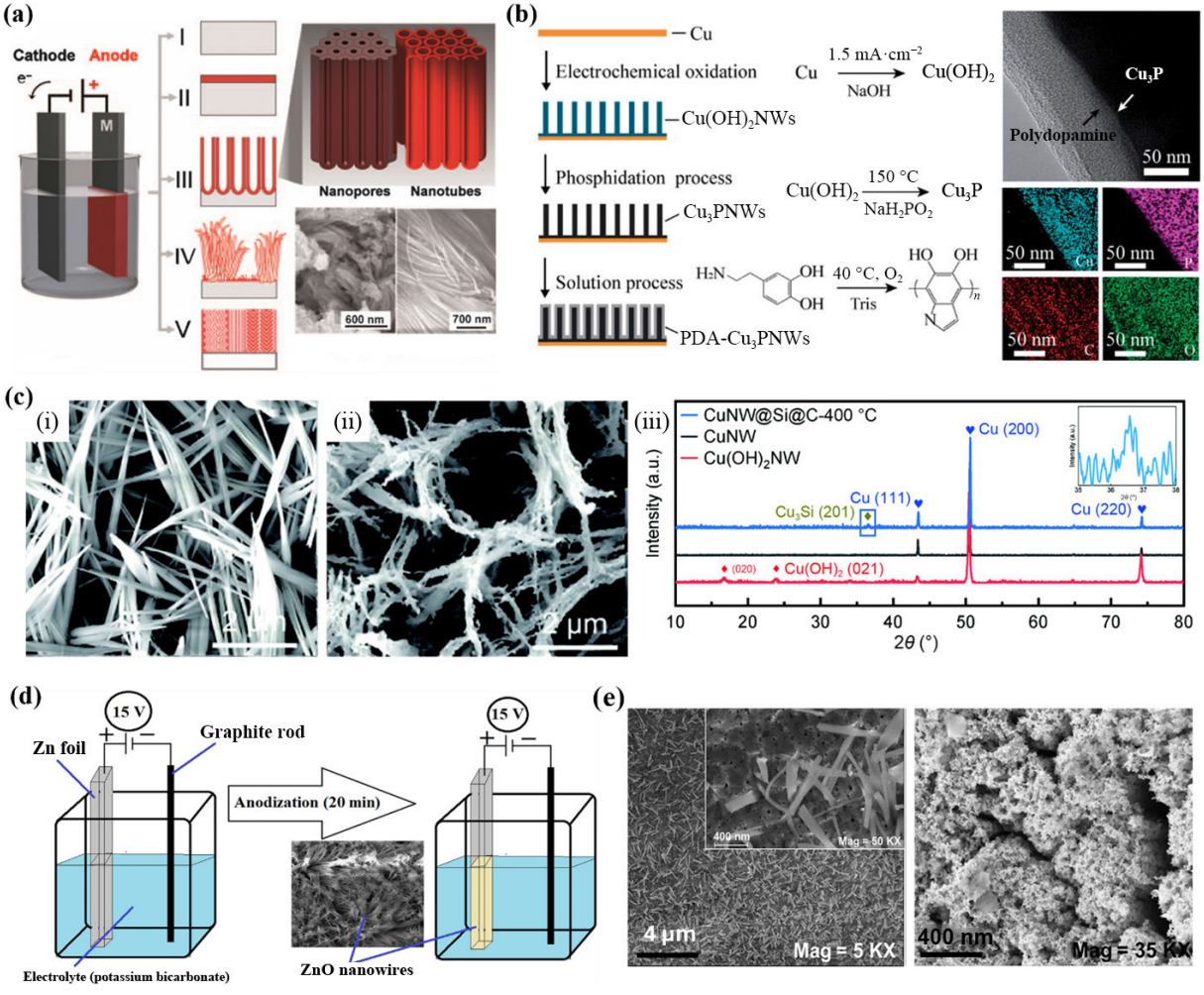

Figure 8 EC anodizing. (a) Schematic illustration of EC anodizing processes. Reproduced with permission from Ref. [139], © WILEY-VCH Verlag GmbH & Co. KGaA, Weinheim 2011. (b) Schematic illustration of the synthesis of PDA-coated Cu_3PNWs on copper foam (left), and TEM image and the corresponding element mapping pattern. Reproduced with permission from Ref. [143], © Royal Society of Chemistry 2019. (c) SEM images of $Cu(OH)_2$ nanowires (i), CuNWs (ii), and XRD patterns of these nanowires (iii). Reproduced with permission from Ref. [144], © Tsinghua University Press 2023. (d) Schematic illustration of the synthesis of ZnONWs and SEM image of ZnONWs. Reproduced with permission from Ref. [145], © Elsevier B.V. 2020 (e) FESEM images of ZnONWs anodized under voltages of 30 V (left) and 20 V (right). Reproduced with permission from Ref. [146], © Elsevier B.V. 2021.

$$ZnO(s) + 2F^-(aq) + H_2O \rightarrow ZnF_2(s) + 2OH^-(aq) \quad (7)$$

$$ZnF_2(s) \rightarrow Zn^{2+}(aq) + 2F^-(aq) \quad (8)$$

$$Zn^{2+}(aq) + 2OH^-(aq) \rightarrow ZnO(s) + H_2O \quad (9)$$

Notably, an alkali condition is typically required to provide an ample supply of hydroxide ions for the synthesis of anchored nanowires. Moreover, electrochemical anodizing is exclusively viable for conductive materials like electrodeposition, and further modifications are typically required after anodizing due to the metastability of obtained hydroxide nanowires. Furthermore, electrochemical anodizing necessitates precise control over the applied potential or current, which limits its utility in the synthesis of anchored nanowires.

2.6 Chemical precipitation

A classical method of chemical precipitation involves the growth of $Cu(OH)_2$ nanowires by surface oxidation of a copper substrate in an alkaline solution containing ammonium persulfate (APS), as illustrated in Eq. (10) and Fig. 9(a) [147].

$$Cu + 4NaOH + (NH_4)_2S_2O_8 \rightarrow Cu(OH)_2 + 2Na_2SO_4 + 2NH_3\uparrow + 2H_2O \quad (10)$$

The underlying mechanism, to some extent, is similar to EC anodizing, but the oxidation of the substrate is driven by an oxidizing agent (i.e., APS) instead of anodic voltages. Notably, although $Cu(OH)_2$ nanowires are not inherently stable enough for direct use in electrochemical applications—owing to their propensity to transform into CuO nanocrystallites—this technique is adaptable for subsequent modifications, making it a cornerstone for contemporary synthesis of copper-based nanowires [147]. For example, Huo et al. employed this method to fabricate $Cu(OH)_2$ nanowires, followed by converting them into Cu-Hexahydroxytriphenylene (HHTP) nanowires (i.e., a kind of MOF-driven material) through a solvothermal method [148]. Similarly, Ma et al. and Mou et al. immersed copper foil in a solution with 2.6 M NaOH and 0.13 M $(NH_4)_2S_2O_8$ to synthesize $Cu(OH)_2$ nanowires, followed by electrochemical reduction to obtain CuNWs for electrocatalytic reduction of CO_2 (Fig. 9(b)) [17, 43]. Wang group immersed copper foam in a solution with 1 M NaOH and 0.1 M $(NH_4)_2S_2O_8$ for 1 h under ambient conditions, followed by ion exchange, annealing, and electrochemical reduction to obtain Ru-dispersed CuNWs (Fig. 9(c)) [16]. Moreover, Chen et al. prepared a solution with 6 M NaOH and 1.2 M $(NH_4)_2S_2O_8$ to etch copper foam and coated with CoNi layered double hydroxides (LDH) through electrodeposition using $Co(NO_3)_2$ and $Ni(NO_3)_2$ as the electrolyte [149]. In Chen's paper, the authors claimed to obtain CuONWs directly after the chemical

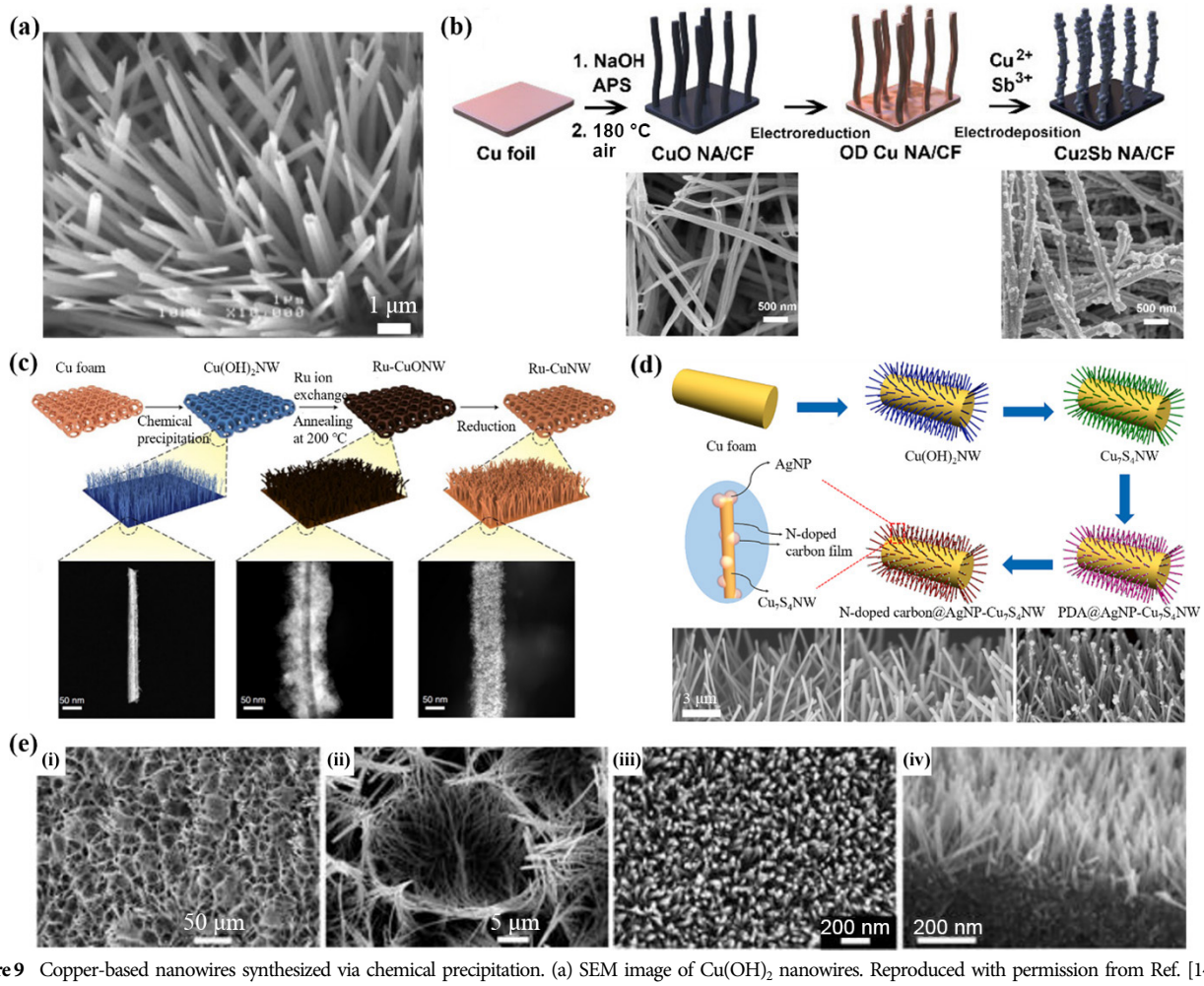

Figure 9 Copper-based nanowires synthesized via chemical precipitation. (a) SEM image of $Cu(OH)_2$ nanowires. Reproduced with permission from Ref. [147], © WILEY-VCH Verlag GmbH & Co. KGaA, Weinheim 2003. (b) Schematic illustration of the synthesis of Cu_2Sb-CuNWs and corresponding SEM images for the second and fourth step. Reproduced with permission from Ref. [17], © Tsinghua University Press and Springer-Verlag GmbH Germany, part of Springer Nature 2021. (c) Schematic illustration of the synthesis of Ru-CuNWs and corresponding STEM images for each step. Reproduced with permission from Ref. [16], © Chen, F. Y. et al., under exclusive license to Springer Nature Limited 2022. (d) Schematic illustration of the synthesis of N-doped carbon coated Ag-Cu_7S_4NWs and corresponding STEM images for each step (from left to right). Reproduced with permission from Ref. [70], © Elsevier Inc. 2023. (e) SEM images of ZnONWs grown at 150 °C ((i) and (ii)) and room temperature ((iii) and (iv)) for 2 days. Reproduced with permission from Ref. [153], © Royal Society of Chemistry 2006.

precipitation as mentioned in the experimental section [149]. This assertion may be incorrect, or it is possible that an annealing step, which should have occurred between the chemical precipitation and electrodeposition steps, was inadvertently omitted. Notably, in the first step to obtaining $Cu(OH)_2$ nanowires, the concentration of hydroxide ions is required to be higher than 1 M, or $Cu_4(SO_4)(OH)_6$ instead of $Cu(OH)_2$ would form, as described in Eq. (11) [147, 149].

$$Cu + 14OH^- + 4(NH_4)_2S_2O_8 \rightarrow Cu_4(SO_4)(OH)_2 + 7SO_4^{2-} + 8NH_3 \uparrow \quad (11)$$

Furthermore, some studies also conducted this chemical precipitation process at a low temperature, which may minimize the temperature gradients near the surface and thus improve etch uniformity across the substrate surface [150]. Yu et al. subjected copper foil to treatment with 2.67 M NaOH and 0.133 M $(NH_4)_2S_2O_8$ at 5 °C for 15 min, followed by annealing the as-prepared copper foil with anchored $Cu(OH)_2$ nanowires in air at the temperature ranging from 150 to 250 °C to obtain Cu_xO nanowires (Cu_xONWs, x represents the degree of crystallinity) [58]. Chen group etched a copper foam at 4 °C for 10 min and annealed it at 180 °C for 3 h to obtain CuONWs or Cu_2ONWs [73, 151, 152]. Then the copper foam with anchored copper/cuprous oxide nanowires was decorated with AgNPs and carbon layer or further converted into Cu_7S_4 nanowires (Cu_7S_4NWs), enhancing the performance and stability of the electrodes (Fig. 9(d)) [23, 70, 151]. Interestingly, although many studies have annealed $Cu(OH)_2$ nanowires to yield CuONWs, the possibility of forming Cu_2ONWs or Cu_xONWs as final products has been demonstrated [58, 73, 152]. This phenomenon underscores the critical importance of meticulously controlling the annealing temperature and conducting comprehensive characterization of the final products to ensure accuracy and reliability.

In addition to copper-based nanowires, this chemical precipitation process has proven effective for synthesizing ZnONWs on zinc substrates. Lu et al. discovered that immersing zinc foil in a solution of APS and NaOH at elevated temperatures resulted in the formation of honeycomb-like micro-patterned ZnONW arrays (Fig. 9(e)) [153]. Similarly, Luo et al. treated zinc foil with NaOH and APS, followed by autoclaving at 150 °C for 2 h, to synthesize ZnONWs with potential applications in CO_2 reduction [154]. Here, we still classify these processes as chemical precipitation rather than solvothermal growth because the procedures involved an etchant (i.e., APS) rather than a precursor (e.g., $ZnCl_2$ and $Zn(NO_3)_2$), and the precipitation process could still perform at room temperatures [153]. However, while chemical precipitation offers a viable route for producing ZnONWs, research in this area remains relatively limited. In contrast, solvothermal growth techniques, which utilize seeds and precursors, have been more extensively developed and have become the predominant methodology for the synthesis of anchored ZnONWs, as elaborated in Section 2.3.

2.7 Metal-assisted chemical etching

Different from various bottom-up approaches as introduced above, MACE provides a highly controllable and economically advantageous top-down alternative for the synthesis of various silicon nanowires (SiNWs), garnering significant interest over the last decade [155–157]. The phenomenon of MACE was first reported in 1997, with Li and Bohn later conducting a systematic exploration that established MACE as a prevalent technique [158, 159]. In a typical MACE process, a noble metal catalyst, such as gold and silver, is initially deposited onto the silicon substrate. This deposition can be achieved through various techniques, including e-beam evaporation [160], electrodeposition [161], and sputtering [162], mirroring the initial phase of VLS growth. Subsequently, an etchant composed of HF and an oxidizing agent, typically H_2O_2, is applied to the silicon substrate. The area beneath the noble metal is etched faster than the area without metal coverage because the chemical reaction occurs preferentially adjacent to the noble metal catalyst, as illustrated in Eqs. (12)–(14) and Fig. 10(a) [156]. HF is preferred because it specifically attacks the silicon dioxide layer without excessively oxidizing the silicon, enabling a controlled etching process when combined with an appropriate oxidizing agent like H_2O_2. Prior reviews have elucidated the intricate mechanisms underlying MACE, such as hole injection, charge transfer, the pivotal role of the metal catalyst, and aspects of mass transfer [156].

$$\text{Cathode reaction}: H_2O_2 + 2H^+ \rightarrow 2H_2O + 2h^+ (\text{holes}) \quad (12)$$

$$\text{Anode reaction}: Si + 2H_2O \rightarrow SiO_2 + 4H^+ + 4e^- \quad (13)$$

$$\text{Dissolution}: SiO_2 + 6HF \rightarrow H_2SiF_6 + 2H_2O \quad (14)$$

Pérez-Díaz et al. implemented UV lithography to pattern a silicon wafer before MACE, followed by an over-etching step using a potassium hydroxide (KOH) solution to refine the structural integrity of SiNWs for LIBs [163]. Yeom et al. employed nanosphere lithography (NSL) for the deposition of gold catalysts onto the silicon wafer, followed by MACE to decouple diameter and pitch in SiNW arrays, extending the types and quality of SiNWs (Fig. 10(b)) [164]. Mishra et al. employed electro-less deposition of silver by immersing silicon wafer in the solution composed of $AgNO_3$ and HF for 1 min under ambient conditions, followed by MACE using HF and H_2O_2 [165]. SiNWs were subsequently decorated with carbon quantum dots (CQDs) to improve the performance of SiNW-anchored silicon wafers in solar cells (Fig. 10(c)) [165]. While most MACE methodologies closely follow the standard procedure—initiating with the deposition of a noble metal such as silver, followed by etching with HF and H_2O_2—the distinct deposition methods underscore the versatility and adaptability of MACE. In addition, as an alternative synthesis for SiNWs, MACE has the advantages of simplicity, cost-effectiveness, and a clean substrate surface resulting from the simple redox process during etching [166]. The anisotropic etch profile also allows MACE to obtain vertically aligned SiNWs with high aspect ratios, potentially enhancing the performance in EFT [11, 166]. Nevertheless, it is noteworthy that the application of MACE has been predominantly confined to the synthesis of SiNWs and has not yet been as extensively applied across the broader domains of electrochemical and electrophysical fields as vapor phase or solvothermal growth methods.

In recent advancements, the scope of MACE has been extended beyond traditional SiNWs. Najar group deposited platinum on GaN and InGaN substrates via sputtering, followed by MACE using HF, H_2O_2, and methanol under UV illumination (Fig. 10(d)) [167, 168]. Similarly, Soopy et al. deposited silver on sulfur-doped InP substrates and applied MACE using H_2SO_4 and H_2O_2 under UV illumination [169]. However, the etching mechanisms in these studies were different from conventional MACE mechanisms. In these examples, the photo-dissolution of the semiconductor substrates (e.g., GaN and InP) occurs by using UV illumination to create electron-hole pairs. The deposited noble metal served as a masking agent that inhibits, rather than facilitates, the etching process [169]. These findings may expand the potential applications for MACE, highlighting the possibility of its utilization across a more diverse set of substrate materials.

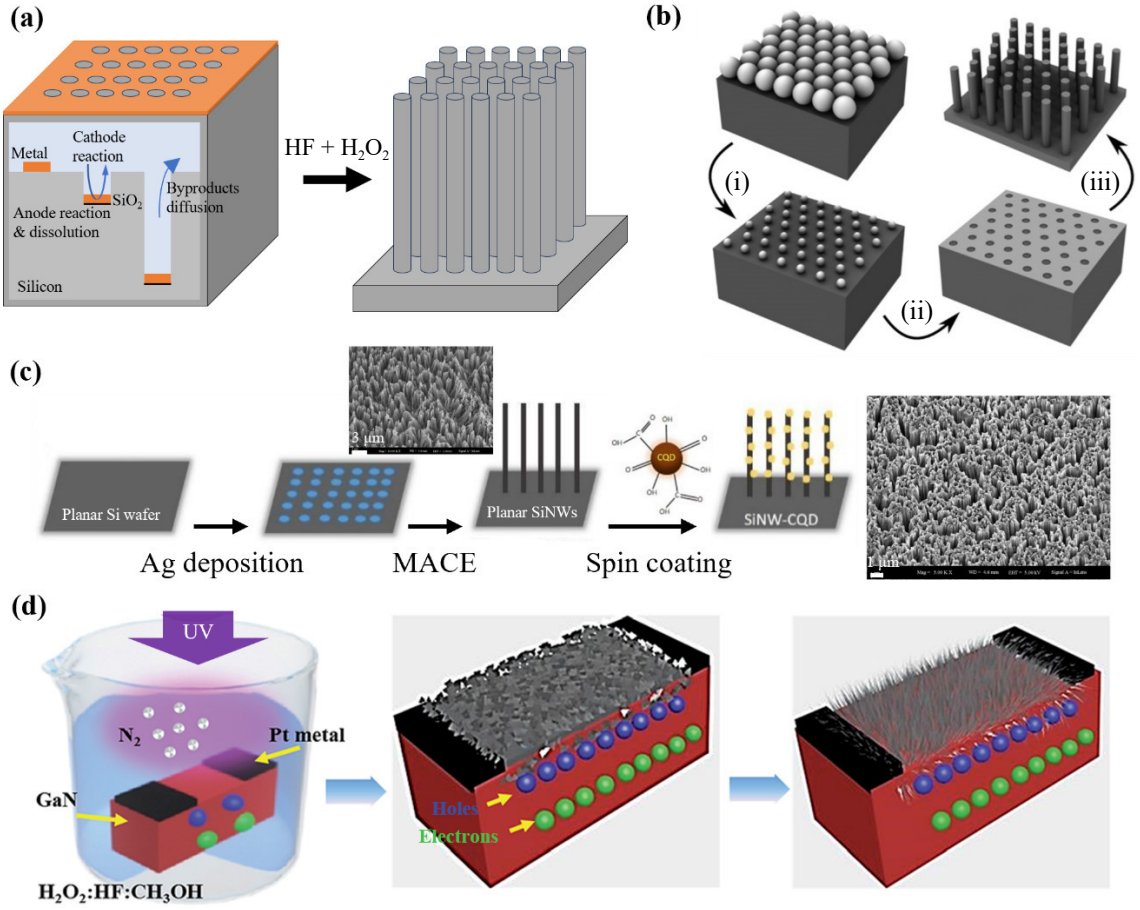

Figure 10 Metal-assisted chemical etching (MACE). (a) Schematic illustration of MACE: hydrogen peroxide is reduced to water (cathode reaction), silicon substrate is oxidized to SiO_2 and subsequently dissolved by hydrofluoric acid (anode reaction & dissolution). (b) Schematic illustration of the synthesis of SiNWs using NSL and MACE: Polystyrene nanospheres (PS NSs) was spin-coated on silicon wafer, NSs were etched in an ICP-RIE with a mixture of O_2 and CF_4 (i), gold was evaporated on Si wafer topped with NS array, followed by NS dissolution (ii), MACE using HF, H_2O_2, and ethanol (iii). Reproduced with permission from Ref. [164], © WILEY-VCH Verlag GmbH & Co. KGaA, Weinheim 2013. (c) Schematic illustration of the synthesis of CQD-SiNWs on silicon wafer and corresponding SEM images for last two steps. Reproduced with permission from Ref. [165], © Elsevier Ltd. 2023. (d) Schematic illustration of the synthesis of GaN nanowires using UV-based MACE. Reproduced from Ref. [168], © Najar, A. et al. 2017.

3 Modification of anchored nanowires

Recent progress in the domain of anchored nanowires for electrochemical and electrophysical applications is concisely summarized in Table 1. This summary reveals that, alongside the advancements in materials science, there is a marked trend toward the extensive investigation of nanowire post-synthesis modifications. These modifications can be categorized into three primary strategies: chemical conversion, functional coatings, and the integration with QDs or NPs, as shown in Fig. 11. The objectives underlying these modifications are multifaceted, aiming to enhance the composite structure of nanowires, increase their mechanical robustness, improve electrical conductivity, and/or boost their capacity or electrocatalytic performance. These objectives and the methodologies employed to achieve them are elaborated upon in the subsequent sections.

3.1 Chemical conversion

Chemical conversion of nanowires encompasses a suite of techniques designed to alter the composition and properties of pre-formed nanowires through methods including reduction, annealing, or ion exchange. Reduction, particularly, is frequently utilized for the modification of copper-based nanowires, enabling the transformation of CuONW into CuNW via thermal and/or an electrochemical approach (Figs. 9(b) and 9(c)). This transformation endows CuNWs with several advantageous properties over CuONWs: (1) enhanced catalytic activity beneficial for diverse electrochemical reactions, (2) an increase in active sites due to the absence of oxygen atoms on the surface, (3) improved electrical conductivity to facilitate electron transfer, and (4) superior electrochemical stability to resist dissolution or reduction [170]. These merits allow CuNWs to have a broad application such as electrocatalytic CO_2 reduction [44, 46]. The methodologies for achieving CuNWs, including both hydrogen and electrochemical reduction, present nuances that merit closer examination. For example, Wang et al. observed that the

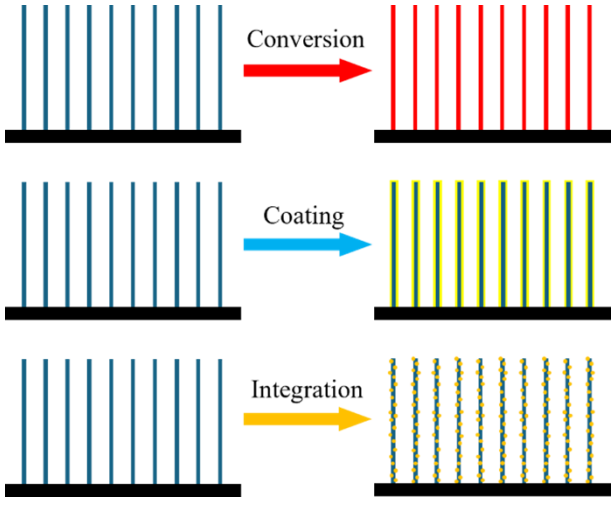

Figure 11 Schematics illustration of three types of modifications.

combinations of hydrogen and electrochemical reduction resulted in different grain boundary densities in CuNWs, subsequently influencing their catalytic activities (Fig. 3(d)) [46]. Specifically, an increase in grain boundary density correlated with heightened catalytic activity toward CO_2 reduction over HER, yielding syngas with a desirable low H_2/CO ratio [46]. Raciti et al. explored three methods to obtain CuNWs: electrochemical reduction at –0.4 V, and hydrogen reduction under 150 and 300 °C [44]. Their findings revealed that electrochemically reduced nanowires typically possessed diameters ranging from 50 to 100 nm and lengths up to 50 μm, whereas nanowires reduced at lower temperatures exhibited similar lengths but marginally larger diameters (i.e., 100 to 120 nm). Conversely, nanowires subjected to high-temperature reduction demonstrated greater diameters (i.e., > 200 nm) and reduced lengths (i.e., ~ 20 μm), likely a result of thermally induced atomic diffusion and the growth of crystalline domains [44]. Furthermore, each type of CuNWs displayed distinctive catalytic activities for CO_2 reduction, leading to the formation of varied products such as CO, HCOOH, or ethanol [44]. These investigations into CuNWs unveil the intricate relationship between processing conditions and the resulting nanowire characteristics, enhancing our understanding of the thermal and electrochemical reductions of CuONWs.

Annealing emerges as a pivotal modification technique for nanowire technology, primarily aimed at improving the crystallinity of nanowires by mitigating defects and dislocations within their crystal lattice [171]. This process is particularly instrumental to $Cu(OH)_2$ nanowires, synthesized by EC anodizing or alkaline chemical precipitation. Copper hydroxide, characterized by its metastable structure where each oxygen atom is coordinatively bonded to two copper atoms and a single hydrogen atom, undergoes a significant transformation upon exposure to temperatures exceeding 150 °C. This thermal exposure results in the dehydration of $Cu(OH)_2$ to CuO, during which an O–Cu–O bridge forms between the previous layers of $Cu(OH)_2$ (Fig. 12) [172, 173]. This transition not only illustrates the structural evolution from $Cu(OH)_2$ to CuO but also underscores the elevated stability in CuO, where each oxygen atom is surrounded by four copper atoms [172]. Hence, many studies have focused on annealing $Cu(OH)_2$NWs to produce CuONWs for diverse applications [58, 73, 149, 151, 152, 174]. However, as mentioned in Section 2.6, the annealing process might lead to the formation of Cu_2ONWs or Cu_xONWs, depending on the degree of crystallization. Furthermore, annealing plays a crucial role in purifying nanowires post-solvothermal synthesis [171]. The solvothermal method, while effective for nanowire formation, often results in the incorporation of impurities such as unreacted precursors, byproducts, or solvent residues within the nanowire structure or on its surface. Annealing facilitates the diffusion or reaction of these impurities with the ambient environment, thereby purging them from the nanowires. The precise parameters of the annealing process, typically set between 300–500 °C for several hours, are meticulously calibrated to maximize impurity removal while concurrently preserving the integrity of the nanowires [15, 115, 118–120].

In addition to reduction and annealing techniques, ion exchange represents a critical strategy for enhancing the functional properties of nanowires. This method, as summarized in Table 1, frequently employs phosphorus and sulfur for their propensity to form stable compounds with a broad array of metals and semiconductors. For example, the calcination of NaH_2PO_2 powder in an argon atmosphere at temperatures ranging from 300 to 350 °C with pre-formed nanowires facilitates the synthesis of CoPNWs [60], Cu_3PNWs (Fig. 8(b)) [142], and Mo-Fe-Ni-P nanowires [121]. In parallel, employing a Na_2S solution in

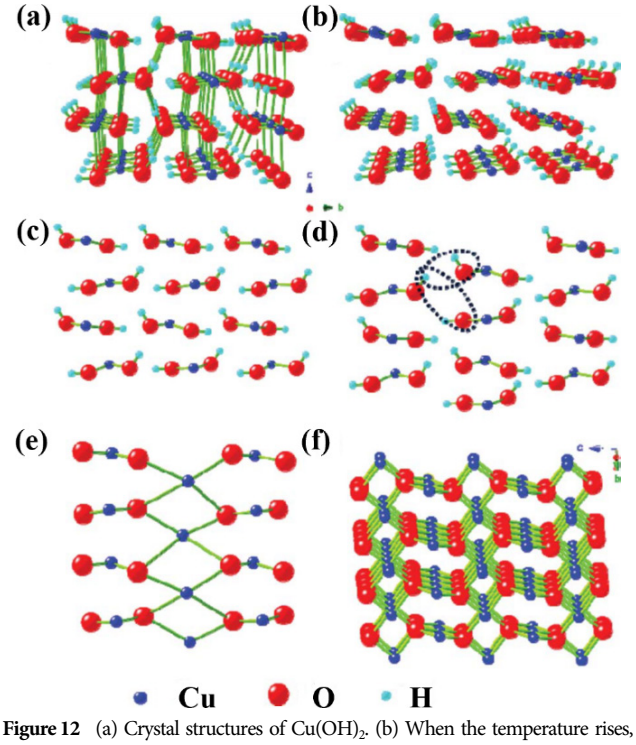

Figure 12 (a) Crystal structures of $Cu(OH)_2$. (b) When the temperature rises, long Cu–O bonds break and H–O bonds break. The structure of $Cu(OH)_2$ changes to a layered $Cu(OH)_4$ structure. (c) Projection along the *a*-axis for (b). (d) and (e) The dehydration process in the *b*, *c* plane of $Cu(OH)_2$. (f) Crystal structure of CuO. Reproduced with permission from Ref. [173], © Royal Society of Chemistry 2012.

autoclave conditions at 90 to 120 °C to the substrates with anchored nanowires yields various nanowires, including $NiCo_2S_4$ nanowires [59], ZnCoS nanowires [65], Co_3S_4NWs (Fig. 5(c)) [22], and Cu_7S_4NWs (Fig. 9(d)) [23, 70]. Transition-metal phosphides (TMPs) and transition-metal chalcogenides (TMCs) are distinguished by their metalloid characteristics and enhanced electrical conductivity, which is beneficial for electron transfer and the diffusion of reactants through the electrolyte [59, 60]. Moreover, TMPs and TMCs have the advantages of low cost, environmental friendliness, and low electronegativity, which are considered promising alternatives to electrocatalysis, such as HER and OER [175–177]. Cu_3PNW also exhibited improved electrochemical stability, extending the operational lifespan of the electrodes with anchored nanowires in EFT applications [142]. Beyond phosphorus and sulfur, Ji et al. autoclaved Co(OH)F nanowires with Na_2TeO_3 and N_2H_4 solution at 180 °C for 15 h to synthesize $CoTe_2$NWs [57]. The introduction of tellurium not only enhanced catalytic kinetics toward OER but also led to superior mass transport properties and mechanical robustness [57]. Akin TMCs, the comparative advantages of $CoTe_2$NWs over Co(OH)F nanowires are likely attributed to the decrease of electronegativity from oxygen to tellurium, resulting in improved metallic characteristics that facilitate transmission in metal chalcogenides [178].

Lastly, titanate (e.g., $K_2Ti_4O_9$) nanowires, with their inherent layered structure, serve as a prominent substrate for modifications through ion exchange processes [179]. In these structures, cations such as Na^+, K^+, and H^+ are situated within the interstices between the layers formed by TiO_6 octahedra, which confers enhanced electrical conductivity predominantly along the direction parallel to the layers [15, 122]. Meanwhile, exchange reactions can be easily carried out with transition-metal ions (e.g., Co^{2+}, Ni^{2+}, Fe^{2+}, and Cu^{2+}), facilitating the entrapment of these ions between the open layers of titanate without altering the interlayer spacing (Fig. 6(a)) [180–182]. This observation underscores the structural

integrity and rigidity of the titanate framework, which remains uncompromised during the ion exchange process. Innovative applications of this principle include the work by Zhao et al., who incorporated iron oxide within TiO_xLNW to act as an OER electrocatalyst [15]. Concurrently, Zhou et al. explored the integration of $Ni(OH)_2$ as a three-dimensional coating to amplify the efficacy of supercapacitors [122]. These modifications not only enhance the functional performance of titanate nanowires in specific electrochemical applications but also illustrate the broader potential of ion exchange as a method for engineering advanced nanostructured materials.

3.2 Functional coating

The functional coating of nanowires entails the strategic application of thin material layers onto the nanowire surface, utilizing techniques such as sputtering [98, 144], chemical bath deposition (CBD) [25, 119, 174], and electrodeposition [123, 149]. This process aims to enhance mechanical strength, prevent electrode corrosion, and bolster the electrochemical performance of nanowires. For example, the application of PDA and carbon coatings has proven effective in mitigating electrochemical reactions during EFT for drinking water and reinforcing the adhesion between nanowires and their substrates, which in turn extends the operational lifespan of electrodes with anchored nanowires for EFT (Figs. 3(a), 8(b), and 9(d)) [73, 95, 143]. Some studies also introduced nitrogen into carbon materials to form N-doped carbon layers, which exhibited higher electronic conductivity, chemical stability, and enhanced electrocatalytic properties [23, 70, 152]. Coatings derived from MOFs are highlighted for their capacity to enhance supercapacitor performance, attributed to their porous structure, efficient electron transfer, and abundant redox sites (Fig. 3(b)) [24, 97, 149]. The advantageous properties of MOF-derived coatings stem from the intricate coordination chemistry of MOFs, which involves metal nodes and diverse organic ligands, thereby facilitating the synthesis of elaborate nanostructures [183].

Additionally, various coatings have been explored to optimize electrodes with anchored nanowires for energy storage and electrocatalysis. Han et al. utilized sputtering to deposit a $NiZn_x$ coating on CuONWs for methanol oxidation. This approach leveraged the high catalytic activity and poisoning resistance of nickel-based materials, while the inclusion of zinc adjusted the electronic structure of nickel for improved performance (Fig. 3(c)) [98]. Su et al. sputtered polysilicon and graphite targets to coat a Si/C layer on CuNWs, aiming to create flexible LIBs (Fig. 8(c)) [144]. Zhao et al. developed a core–shell nanowire to combine $NiCo_2O_4$ (core) with $NiMoO_4$ (shell), which could be considered as a $NiCo_2O_4$ nanowire coated by a $NiMoO_4$ layer [119]. This configuration exploited the synergistic effects between the two materials, tripling the specific capacitance compared to a single-material $NiCo_2O_4$ electrode [119]. Zhou et al. engineered $K_2Ti_4O_9$ nanowires into three-dimensional structures by coating $Ni(OH)_2$ nanosheets on the titanate nanowires, which enhanced the contact interface between the electrolyte and active material in supercapacitors (Fig. 6(b)) [122]. Furthermore, Wang et al. advanced LIB technology by electrodepositing a MoO_3 shell on TiO_2NWs, achieving large reversible capacity and elevated electrical conductivity (Fig. 6(d)) [123]. In conclusion, these innovative approaches to nanowire functionalization underscore the transformative potential of coatings in optimizing the performance and application scope of nanowires with anchored nanowires in EFT, electrocatalysis, and energy storage domains.

3.3 Integration with QDs or NPs

The integration of QDs or NPs into nanowires represents another cutting-edge advancement in nanowire modifications, offering unique opportunities for applications in electrocatalysis and EFT. Gautam et al. decorated ZnCoS nanowires with POM nanoparticles via a solvothermal method to achieve remarkable efficiency in overall water splitting [65]. The enhanced performance of POM-ZnCoS nanowires is attributable to the increased electroactive sites and active surface area due to the insertion of POM nanoparticles [65]. Chen group integrated silver nanoparticles (AgNPs) into copper-based nanowires to elevate their electrical conductivity for EFT of drinking water (Fig. 6(f)) [70, 73, 151]. Similarly, Tian's work, which involved incorporating AgNPs into ZnONWs using a dip-coating and light irradiation method, further exemplifies this strategy for EFT [68]. It is worth mentioning that the intrinsic antibacterial properties of silver potentially enhance the inactivation efficiency during EFT [74, 75].

On the other hand, QDs have found extensive applications in solar cell technologies, primarily due to their tunable band gaps, which allow for the efficient harnessing of the solar spectrum [126]. QDs can also establish a distinct intermediate band within the band gap of the host material, capturing photons with energy below the host material energy gap, or enhancing the photocurrent within solar cells [165]. For example, Wang et al. demonstrated the embedding of PbS QDs within ZnONWs through a two-step process involving chemical deposition (using QD octane solution) and ion exchange (using tetrabutylammonium iodide methanol solution) (Fig. 6(e)) [126]. This integration strategy circumvented the need for electron-blocking layers (EBLs), culminating in solar cells with enhanced power conversion efficiency (PCE) and external quantum efficiency (EQE) [126]. Additionally, Mishra et al. enhanced the performance of SiNWs by spin-coating nitrogen-doped CQDs on them, achieving effective suppression of recombination and improved optical absorption (Fig. 10(c)) [165]. These advancements underscore the transformative impact of integrating QDs and NPs into nanowires, not only enhancing the functional attributes of these nanostructures but also broadening their application scope.

4 Prospects and challenges

The advantages and limitations of various synthesis methodologies have been summarized in Table 2. Specifically, the solvothermal method stands as the predominant choice for fabricating anchored nanowires, particularly those based on cobalt, titanium, and zinc, across a variety of substrates such as nickel foam, titanium foam, graphite felt, and carbon cloth. However, this method requires a long operation time (typically tens of hours) and further modifications (e.g., annealing) to remove impurities such as unreacted precursors, byproducts, or solvent residues. Conversely, thermal oxidation, chemical precipitation, and MACE are time-saving and easy to execute, but each method suffers from its constraints. Thermal oxidation is predominantly applied for metal oxide nanowires, whereas MACE and chemical precipitation are typically suitable for SiNWs and metal hydroxide nanowires, respectively. VLS growth, electrodeposition, and EC anodizing, while offering controlled manipulation over the diameter and density of the nanowires, require complex operational procedures, which increase the risk of undesired reactions. The selection of synthesis methodologies for anchored nanowires intricately depends on their compositional and substrate compatibility. Thermal oxidation, EC anodizing, chemical precipitation, and MACE, for example, are particularly effective for fabricating nanowires that are compositionally identical to their substrates (e.g., metal foil or silicon wafer), whereas solvothermal growth, VLS growth, and electrodeposition excel in the fabrication of heterogeneous nanowires and complex coaxial structures. Moreover, thermal oxidation and VLS growth stand out for their capacity to produce single-crystalline structures,

a characteristic that significantly enhances the electronic properties and carrier mobility of the nanowires.

The methodologies and objectives of various modification approaches have been outlined in Table 3. Briefly, chemical conversion fundamentally alters the composition and, consequently, the characteristics of the nanowires. In contrast, functional coatings and the integration of QDs or NPs augment the original nanowires with additional functionalities, enriching their utility across a spectrum of applications. The ultimate goals of these strategies can be categorized into elevating electrical conductivity to facilitate electron transport, increasing the loading of active materials to improve the capacity or catalytic activity, and fortifying mechanical strength to extend the electrode lifespan. The selection of modification approaches for anchored nanowires depends on the specific requirements of their intended electrochemical or electrophysical applications. For instance, chemical conversion and the integration of NPs emerge as effective strategies for altering or loading nanowires with materials optimized for electrocatalysis and energy storage. Specifically, electrocatalysis demands nanowires capable of supporting materials with superior catalytic efficiency and selectivity toward desired reactions, while energy storage applications such as LIBs necessitate materials that possess a high capacity. For applications in EFT, where the emphasis shifts toward electrochemical stability and mechanical durability, the application of protective coatings becomes essential. Such coatings not only safeguard the nanowires but also enhance their operational lifespan by mitigating degradation risks. Moreover, chemical conversion techniques offer a pathway to transform the original nanowire materials into variants that are inherently more inert or exhibit improved corrosion resistance.

On the other hand, the progression of anchored nanowire technologies encounters several hurdles that necessitate focused attention and innovative solutions. Firstly, the translation of anchored nanowire synthesis from the laboratory to the industrial scale is fraught with challenges, including the excessive cost of production, resource-demanding synthesis procedures, and the prerequisite for specialized fabrication equipment. This transition urgently requires the innovation of scalable and cost-efficient fabrication methodologies to facilitate commercial viability. Secondly, enhancement in stability and resilience of electrodes with anchored nanowires in real-world operational settings poses significant concerns. Degradative phenomena, including structural disintegration, surface oxidation, and detachment from their substrates critically undermine the long-term functionality and reliability of these devices. It is imperative to pioneer the development of durable, corrosion-resistant materials alongside advanced protective coatings to enhance their applicability in practical settings. Lastly, the broader environmental and health ramifications associated with the lifecycle of nanowires—from production and use to disposal—are yet to be fully elucidated. Concerns over the potential ecological release, bioaccumulation, and cytotoxic effects of nanowires call for thorough lifecycle analyses, alongside the establishment of rigorous protocols for their safe handling, application, and recycling. Furthermore, it is vital to address the environmental footprint of chemical wastes generated during solvothermal synthesis, electrochemical techniques, and etching processes through meticulous collection and disposal practices. These challenges underscore the need for a multidisciplinary approach, combined with insights from materials science, engineering, environmental studies, and toxicology, to navigate the path toward sustainable and safe nanowire technologies.

5 Conclusion

In this comprehensive review, we have explored the landscape of electrodes with anchored nanowires tailored for electrochemical and electrophysical applications that have emerged over the past decade. We have underscored seven synthesis methodologies (i.e., thermal oxidation, VLS growth, solvothermal growth, electrodeposition, EC anodizing, chemical precipitation, and MACE) and five modification approaches (i.e., chemical conversion, functional coatings, and the integration with QDs/NPs). For nanowire synthesis, VLS growth, solvothermal growth, electrodeposition, and EC anodizing are more compatible and controllable. Conversely, thermal oxidation, chemical precipitation, and MACE are lauded for their simplicity and potential for scalability. The selection of synthesis methodologies for anchored nanowires intricately depends on their compositional and substrate compatibility. For nanowire modification, chemical conversion fundamentally alters the composition of the nanowires, whereas functional coatings and the integration of QDs or NPs augment the original nanowires with additional functionalities. The objectives of the modification techniques are to improve electrical conductivity, augment active material loading, and bolster mechanical integrity. The selection of modification approaches for anchored nanowires depends on the specific requirements of their intended electrochemical or electrophysical applications. Looking forward, the journey towards the development of anchored nanowires calls for rigorous research focused on assessing the viability of these technologies at an industrial scale, as well as the creation of more durable and environmentally sustainable nanowire systems.

Acknowledgements

We acknowledge the financial support from the National Science Foundation via Grant CBET 2203162. We also acknowledge the suggestions from Jarin Mourin on the grammar and vocabulary of this paper.

References

[1] Xia, Y.; Yang, P.; Sun, Y.; Wu, Y.; Mayers, B.; Gates, B.; Yin, Y.; Kim, F.; Yan, H. One-dimensional nanostructures: Synthesis, characterization, and applications. *Adv. Mater.* **2003**, *15*, 353–389.

[2] Cao, G. Z. *Nanostructures & Nanomaterials*: *Synthesis*, *Properties & Applications*; Imperial College Press: London, **2004**.

[3] Dasgupta, N. P.; Sun, J. W.; Liu, C.; Brittman, S.; Andrews, S. C.; Lim, J.; Gao, H. W.; Yan, R. X.; Yang, P. D. 25th Anniversary article: Semiconductor nanowires-synthesis, characterization, and applications. *Adv. Mater.* **2014**, *26*, 2137–2184

[4] Kuchibhatla, S. V. N. T.; Karakoti, A. S.; Bera, D.; Seal, S. One dimensional nanostructured materials. *Prog. Mater. Sci.* **2007**, *52*, 699–913.

[5] Lieber, C. M. One-dimensional nanostructures: Chemistry, physics & applications. *Solid State Commun.* **1998**, *107*, 607–616.

[6] Li, Y.; Qian, F.; Xiang, J.; Lieber, C. M. Nanowire electronic and optoelectronic devices. *Mater. Today* **2006**, *9*, 18–27.

[7] Tiwari, J. N.; Tiwari, R. N.; Kim, K. S. Zero-dimensional, one-dimensional, two-dimensional and three-dimensional nanostructured materials for advanced electrochemical energy devices. *Prog. Mater. Sci.* **2012**, *57*, 724–803.

[8] Agarwal, R.; Lieber, C. M. Semiconductor nanowires: Optics and optoelectronics. *Appl. Phys. A* **2006**, *85*, 209–215.

[9] Mai, L.; Tian, X. C.; Xu, X.; Chang, L.; Xu, L. Nanowire electrodes for electrochemical energy storage devices. *Chem. Rev.* **2014**, *114*, 11828–11862.

[10] Zhou, G. M.; Xu, L.; Hu, G. W.; Mai, L.; Cui, Y. Nanowires for electrochemical energy storage. *Chem. Rev.* **2019**, *119*, 11042–11109.

[11] Zhou, J. F.; Yu, C.; Wang, T.; Xie, X. Development of nanowire-modified electrodes applied in the locally enhanced electric field treatment (LEEFT) for water disinfection. *J. Mater. Chem. A* **2020**, *8*, 12262–12277.

[12] Ahn, J.; Hwang, H.; Jeong, S.; Moon, J. Metal-nanowire-electrode-based perovskite solar cells: Challenging issues and new opportunities. *Adv. Energy Mater.* **2017**, *7*, 1602751.
[13] Hu, L. B.; Kim, H. S.; Lee, J. Y.; Peumans, P.; Cui, Y. Scalable coating and properties of transparent, flexible, silver nanowire electrodes. *ACS Nano* **2010**, *4*, 2955–2963.
[14] Jiang, J.; Li, Y. Y.; Liu, J. P.; Huang, X. T. Building one-dimensional oxide nanostructure arrays on conductive metal substrates for lithium-ion battery anodes. *Nanoscale* **2011**, *3*, 45–58.
[15] Zhao, L. L.; Cao, Q.; Wang, A. L.; Duan, J. Z.; Zhou, W. J.; Sang, Y. H.; Liu, H. Iron oxide embedded titania nanowires—An active and stable electrocatalyst for oxygen evolution in acidic media. *Nano Energy* **2018**, *45*, 118–126.
[16] Chen, F. Y.; Wu, Z. Y.; Gupta, S.; Rivera, D. J.; Lambeets, S. V.; Pecaut, S.; Kim, J. Y. T.; Zhu, P.; Finfrock, Y. Z.; Meira, D. M. et al. Efficient conversion of low-concentration nitrate sources into ammonia on a Ru-dispersed Cu nanowire electrocatalyst. *Nat. Nanotechnol.* **2022**, *17*, 759–767.
[17] Mou, S. Y.; Li, Y. H.; Yue, L. C.; Liang, J.; Luo, Y. L.; Liu, Q.; Li, T. S.; Lu, S. Y.; Asiri, A. M.; Xiong, X. L. et al. Cu_2Sb decorated Cu nanowire arrays for selective electrocatalytic CO_2 to CO conversion. *Nano Res.* **2021**, *14*, 2831–2836.
[18] Kotnik, T.; Bobanović, F.; Miklavčič, D. Sensitivity of transmembrane voltage induced by applied electric fields-a theoretical analysis. *Bioelectrochem. Bioenerg.* **1997**, *43*, 285–291.
[19] Kotnik, T.; Frey, W.; Sack, M.; Haberl Meglič, S.; Peterka, M.; Miklavčič, D. Electroporation-based applications in biotechnology. *Trends Biotechnol.* **2015**, *33*, 480–488.
[20] Wang, T.; Brown, D. K.; Xie, X. Operando investigation of locally enhanced electric field treatment (LEEFT) harnessing lightning-rod effect for rapid bacteria inactivation. *Nano Lett.* **2022**, *22*, 860–867.
[21] Wang, T.; Xie, X. Nanosecond bacteria inactivation realized by locally enhanced electric field treatment. *Nat. Water* **2023**, *1*, 104–112
[22] Huo, W. C.; Zhang, X. Y.; Liu, X. Y.; Liu, H.; Zhu, Y. M.; Zhang, Y.; Ji, J. Y.; Dong, F.; Zhang, Y. X. Construction of advanced 3D Co_3S_4@PPy nanowire anchored on nickel foam for high-performance electrochemical energy storage. *Electrochim. Acta* **2020**, *334*, 135635
[23] Cui, S. G.; Chen, S. G.; Wang, H. Y.; Dong, L. T.; Wang, S. T. N-doped carbon-coated Cu_7S_4 nanowires on Cu foam supports for water disinfection. *ACS Appl. Nano Mater.* **2021**, *4*, 6124–6134.
[24] Poudel, M. B.; Lohani, P. C.; Acharya, D.; Kandel, D. R.; Kim, A. A.; Yoo, D. J. MOF derived hierarchical ZnNiCo-LDH on vapor solid phase grown Cu_xO nanowire array as high energy density asymmetric supercapacitors. *J. Energy Storage* **2023**, *72*, 108220.
[25] Chebrolu, V. T.; Balakrishnan, B.; Cho, I.; Bak, J. S.; Kim, H. J. A unique core–shell structured ZnO/NiO heterojunction to improve the performance of supercapacitors produced using a chemical bath deposition approach. *Dalton Trans.* **2020**, *49*, 14432–14444.
[26] Wang, Y.; Cao, G. Z. Developments in nanostructured cathode materials for high-performance lithium-ion batteries. *Adv. Mater.* **2008**, *20*, 2251–2269.
[27] Peng, K. Q.; Wang, X.; Li, L.; Hu, Y.; Lee, S. T. Silicon nanowires for advanced energy conversion and storage. *Nano Today* **2013**, *8*, 75–97.
[28] Leveau, L.; Laïk, B.; Pereira-Ramos, J. P.; Gohier, A.; Tran-Van, P.; Cojocaru, C. S. Cycling strategies for optimizing silicon nanowires performance as negative electrode for lithium battery. *Electrochim. Acta* **2015**, *157*, 218–224.
[29] Sandu, G.; Coulombier, M.; Kumar, V.; Kassa, H. G.; Avram, I.; Ye, R.; Stopin, A.; Bonifazi, D.; Gohy, J. F.; Leclère, P. et al. Kinked silicon nanowires-enabled interweaving electrode configuration for lithium-ion batteries. *Sci. Rep.* **2018**, *8*, 9794
[30] Wang, B.; Ryu, J.; Choi, S.; Zhang, X. H.; Pribat, D.; Li, X. L.; Zhi, L. J.; Park, S.; Ruoff, R. S. Ultrafast-charging silicon-based coral-like network anodes for lithium-ion batteries with high energy and power densities. *ACS Nano* **2019**, *13*, 2307–2315
[31] Zhang, L.; Zhang, G. Q.; Wu, H. B.; Yu, L.; Lou, X. W. Hierarchical tubular structures constructed by carbon-coated SnO_2 nanoplates for highly reversible lithium storage. *Adv. Mater.* **2013**, *25*, 2589–2593.
[32] Li, Y. G.; Tan, B.; Wu, Y. Y. Mesoporous Co_3O_4 nanowire arrays for lithium ion batteries with high capacity and rate capability. *Nano Lett.* **2008**, *8*, 265–270.
[33] Hu, J. K.; Sun, C. F.; Gillette, E.; Gui, Z.; Wang, Y. H.; Lee, S. B. Dual-template ordered mesoporous carbon/Fe_2O_3 nanowires as lithium-ion battery anodes. *Nanoscale* **2016**, *8*, 12958–12969.
[34] Yuan, Z. Q.; Si, L. L.; Wei, D. H.; Hu, L.; Zhu, Y. C.; Li, X. N.; Qian, Y. T. Vacuum topotactic conversion route to mesoporous orthorhombic MoO_3 nanowire bundles with enhanced electrochemical performance. *J. Phys. Chem. C* **2014**, *118*, 5091–5101.
[35] Wang, J. X.; Zhang, Q. B.; Li, X. H.; Zhang, B.; Mai, L.; Zhang, K. L. Smart construction of three-dimensional hierarchical tubular transition metal oxide core/shell heterostructures with high-capacity and long-cycle-life lithium storage. *Nano Energy* **2015**, *12*, 437–446.
[36] Xia, H.; Wan, Y. H.; Assenmacher, W.; Mader, W.; Yuan, G. L.; Lu, L. Facile synthesis of chain-like $LiCoO_2$ nanowire arrays as three-dimensional cathode for microbatteries. *NPG Asia Mater.* **2014**, *6*, e126–e126.
[37] Cao, J. H.; Guo, S. W.; Yan, R. Y.; Zhang, C.; Guo, J. L.; Zheng, P. Carbon-coated single-crystalline $LiMn_2O_4$ nanowires synthesized by high-temperature solid-state reaction with high capacity for Li-ion battery. *J. Alloys Compd.* **2018**, *741*, 1–6.
[38] An, Q.; Wei, Q. L.; Zhang, P. F.; Sheng, J. Z.; Hercule, K. M.; Lv, F.; Wang, Q. Q.; Wei, X. J.; Mai, L. Three-dimensional interconnected vanadium pentoxide nanonetwork cathode for high-rate long-life lithium batteries. *Small* **2015**, *11*, 2654–2660.
[39] Zhang, Y.; Lai, J. Y.; Gong, Y. D.; Hu, Y. M.; Liu, J.; Sun, C. W.; Wang, Z. L. A safe high-performance all-solid-state lithium-vanadium battery with a freestanding V_2O_5 nanowire composite paper cathode. *ACS Appl. Mater. Interfaces* **2016**, *8*, 34309–34316.
[40] Hua, K.; Li, X. J.; Fang, D.; Yi, J. H.; Bao, R.; Luo, Z. P. Electrodeposition of high-density lithium vanadate nanowires for lithium-ion battery. *Appl. Surf. Sci.* **2018**, *447*, 610–616.
[41] Shao, Q.; Lu, K. Y.; Huang, X. Q. Platinum group nanowires for efficient electrocatalysis. *Small Methods* **2019**, *3*, 1800545.
[42] Kim, M. J.; Cruz, M. A.; Yang, F. C.; Wiley, B. J. Accelerating electrochemistry with metal nanowires. *Curr. Opin. Electrochem.* **2019**, *16*, 19–27.
[43] Ma, M.; Djanashvili, K.; Smith, W. A. Controllable hydrocarbon formation from the electrochemical reduction of CO_2 over Cu nanowire arrays. *Angew. Chem., Int. Ed.* **2016**, *55*, 6680–6684.
[44] Raciti, D.; Mao, M.; Park, J. H.; Wang, C. Mass transfer effects in CO_2 reduction on Cu nanowire electrocatalysts. *Catal. Sci. Technol.* **2018**, *8*, 2364–2369.
[45] Raciti, D.; Livi, K. J.; Wang, C. Highly dense Cu nanowires for low-overpotential CO_2 reduction. *Nano Lett.* **2015**, *15*, 6829–6835.
[46] Wang, Y. X.; Niu, C. L.; Zhu, Y. C.; He, D.; Huang, W. X. Tunable syngas formation from electrochemical CO_2 reduction on copper nanowire arrays. *ACS Appl. Energy Mater.* **2020**, *3*, 9841–9847.
[47] Li, H. Y.; Wu, X. S.; Tao, X. L.; Lu, Y.; Wang, Y. W. Direct synthesis of ultrathin Pt nanowire arrays as catalysts for methanol oxidation. *Small* **2020**, *16*, 2001135.
[48] Meng, W.; He, H. Y.; Yang, L.; Jiang, Q. G.; Yuliarto, B.; Yamauchi, Y.; Xu, X. T.; Huang, H. J. 1D-2D hybridization: Nanoarchitectonics for grain boundary-rich platinum nanowires coupled with MXene nanosheets as efficient methanol oxidation electrocatalysts. *Chem. Eng. J.* **2022**, *450*, 137932.
[49] Liu, J.; Liu, Z.; Wang, H. Z.; Liu, B.; Zhao, N. Q.; Zhong, C.; Hu, W. B. Designing nanoporous coral-like Pt nanowires architecture for methanol and ammonia oxidation reactions. *Adv. Funct. Mater.* **2022**, *32*, 2110702.
[50] Jiang, X.; Fu, G. T.; Wu, X.; Liu, Y.; Zhang, M. Y.; Sun, D. M.; Xu, L.; Tang, Y. W. Ultrathin AgPt alloy nanowires as a high-performance electrocatalyst for formic acid oxidation. *Nano Res.* **2018**, *11*, 499–510.
[51] Wang, P.; Zhang, Y. Y.; Shi, R.; Wang, Z. H. Trimetallic PtPdCu

nanowires as an electrocatalyst for methanol and formic acid oxidation. *New J. Chem.* **2018**, *42*, 19083–19089.

[52] Zhu, M.; Zhang, Y. Y.; Shi, R.; Wang, Z. H. Ultrathin vein-like iridium-tin nanowires with abundant oxidized tin as high-performance ethanol oxidation electrocatalysts. *Small* **2017**, *13*, 1701295.

[53] Ma, S. Y.; Li, H. H.; Hu, B. C.; Cheng, X.; Fu, Q. Q.; Yu, S. H. Synthesis of low Pt-based Quaternary PtPdRuTe nanotubes with optimized incorporation of Pd for enhanced electrocatalytic activity. *J. Am. Chem. Soc.* **2017**, *139*, 5890–5895.

[54] Jiang, K. Z.; Zhao, D. D.; Guo, S. J.; Zhang, X.; Zhu, X.; Guo, J.; Lu, G.; Huang, X. Q. Efficient oxygen reduction catalysis by subnanometer Pt alloy nanowires. *Sci. Adv.* **2017**, *3*, e1601705.

[55] Huang, H. W.; Li, K.; Chen, Z.; Luo, L. H.; Gu, Y. Q.; Zhang, D. Y.; Ma, C.; Si, R.; Yang, J. L.; Peng, Z. M. et al. Achieving remarkable activity and durability toward oxygen reduction reaction based on ultrathin Rh-doped Pt nanowires. *J. Am. Chem. Soc.* **2017**, *139*, 8152–8159.

[56] Chang, F. F.; Shan, S. Y.; Petkov, V.; Skeete, Z.; Lu, A. L.; Ravid, J.; Wu, J. F.; Luo, J.; Yu, G.; Ren, Y. et al. Composition tunability and (111)-dominant facets of ultrathin platinum-gold alloy nanowires toward enhanced electrocatalysis. *J. Am. Chem. Soc.* **2016**, *138*, 12166–12175.

[57] Ji, L.; Wang, Z. C.; Wang, H.; Shi, X. F.; Asiri, A. M.; Sun, X. P. Hierarchical $CoTe_2$ nanowire array: An effective oxygen evolution catalyst in alkaline media. *ACS Sustain. Chem. Eng.* **2018**, *6*, 4481–4485.

[58] Yu, J.; Cao, Q.; Feng, B.; Li, C. L.; Liu, J. Y.; Clark, J. K.; Delaunay, J. J. Insights into the efficiency and stability of Cu-based nanowires for electrocatalytic oxygen evolution. *Nano Res.* **2018**, *11*, 4323–4332.

[59] Li, X.; Kou, Z. K.; Xi, S. B.; Zang, W. J.; Yang, T.; Zhang, L.; Wang, J. Porous $NiCo_2S_4$/FeOOH nanowire arrays with rich sulfide/hydroxide interfaces enable high OER activity. *Nano Energy* **2020**, *78*, 105230.

[60] Ren, Y. C.; Li, Z. R.; Deng, B.; Ye, C.; Zhang, L. C.; Wang, Y.; Li, T. S.; Liu, Q.; Cui, G. W.; Asiri, A. M. et al. Superior hydrogen evolution electrocatalysis enabled by CoP nanowire array on graphite felt. *Int. J. Hydrogen Energy* **2022**, *47*, 3580–3586.

[61] Liu, Z. J.; Qi, J.; Liu, M. X.; Zhang, S. M.; Fan, Q. K.; Liu, H. P.; Liu, K.; Zheng, H. Q.; Yin, Y. D.; Gao, C. B. Aqueous synthesis of ultrathin platinum/non-noble metal alloy nanowires for enhanced hydrogen evolution activity. *Angew. Chem., Int. Ed.* **2018**, *57*, 11678–11682

[62] Lv, H.; Chen, X.; Xu, D. D.; Hu, Y. C.; Zheng, H. Q.; Suib, S. L.; Liu, B. Ultrathin PdPt bimetallic nanowires with enhanced electrocatalytic performance for hydrogen evolution reaction. *Appl. Catal. B Environ.* **2018**, *238*, 525–532.

[63] Zhang, L. Q.; Liu, L. C.; Wang, H. D.; Shen, H. X.; Cheng, Q.; Yan, C.; Park, S. Electrodeposition of rhodium nanowires arrays and their morphology-dependent hydrogen evolution activity. *Nanomaterials* **2017**, *7*, 103.

[64] Wei, S. T.; Qi, K.; Jin, Z.; Cao, J. S.; Zheng, W. T.; Chen, H.; Cui, X. Q. One-step synthesis of a self-supported copper phosphide nanobush for overall water splitting. *ACS Omega* **2016**, *1*, 1367–1373.

[65] Gautam, J.; Liu, Y.; Gu, J.; Ma, Z. Y.; Zha, J.; Dahal, B.; Zhang, L. N.; Chishti, A. N.; Ni, L. B.; Diao, G. W. et al. Fabrication of polyoxometalate anchored zinc cobalt sulfide nanowires as a remarkable bifunctional electrocatalyst for overall water splitting. *Adv. Funct. Mater.* **2021**, *31*, 2106147.

[66] Liang, Z.; Hou, H. L.; Fang, Z.; Gao, F. M.; Wang, L.; Chen, D.; Yang, W. Y. Hydrogenated TiO_2 nanorod arrays decorated with carbon quantum dots toward efficient photoelectrochemical water splitting. *ACS Appl. Mater. Interfaces* **2019**, *11*, 19167–19175.

[67] Zhou, J.; Hou, H. L.; Fang, Z.; Gao, F. M.; Wang, L.; Chen, D.; Yang, W. Y. Locally enhanced electric field treatment (LEEFT) for water disinfection. *Front. Environ. Sci. Eng.* **2020**, *14*, 78.

[68] Tian, J. J.; Feng, H. Q.; Yan, L.; Yu, M.; Ouyang, H.; Li, H.; Jiang, W.; Jin, Y. M.; Zhu, G.; Li, Z. et al. A self-powered sterilization system with both instant and sustainable anti-bacterial ability. *Nano Energy* **2017**, *36*, 241–249.

[69] Pi, S. Y.; Wang, Y.; Lu, Y. W.; Liu, G. L.; Wang, D. L.; Wu, H. M.; Chen, D.; Liu, H. Fabrication of polypyrrole nanowire arrays-modified electrode for point-of-use water disinfection via low-voltage electroporation. *Water Res.* **2021**, *207*, 117825.

[70] Dong, L. T.; Cui, S. G.; Sun, X.; Liu, J. H.; Lv, G. J.; Chen, S. G. Copper sulfides (Cu_7S_4) nanowires with Ag anchored in N-doped carbon layers optimize interfacial charge transfer for rapid water sterilization. *J. Colloid Interface Sci.* **2024**, *654*, 1209–1219.

[71] Liu, C.; Xie, X.; Zhao, W. T.; Yao, J.; Kong, D. S.; Boehm, A. B.; Cui, Y. Static electricity powered copper oxide nanowire microbicidal electroporation for water disinfection. *Nano Lett.* **2014**, *14*, 5603–5608.

[72] Huo, Z. Y.; Xie, X.; Yu, T.; Lu, Y.; Feng, C.; Hu, H. Y. Nanowire-modified three-dimensional electrode enabling low-voltage electroporation for water disinfection. *Environ. Sci. Technol.* **2016**, *50*, 7641–7649.

[73] Wang, S. T.; Wang, W.; Yue, L. F.; Cui, S. G.; Wang, H. Y.; Wang, C. Y.; Chen, S. G. Hierarchical Cu_2O nanowires covered by silver nanoparticles-doped carbon layer supported on Cu foam for rapid and efficient water disinfection with lower voltage. *Chem. Eng. J.* **2020**, *382*, 122855.

[74] Chen, W. S.; Jiang, J. Y.; Zhang, W. L.; Wang, T.; Zhou, J. F.; Huang, C. H.; Xie, X. Silver nanowire-modified filter with controllable silver ion release for point-of-use disinfection. *Environ. Sci. Technol.* **2019**, *53*, 7504–7512.

[75] Yu, D. M.; Liu, L. F.; Ding, B.; Yu, J. Y.; Si, Y. Spider-Web-Inspired SiO_2/Ag nanofibrous aerogels with superelastic and conductive networks for electroporation water disinfection. *Chem. Eng. J.* **2023**, *461*, 141908.

[76] Kempa, T. J.; Day, R. W.; Kim, S. K.; Park, H. G.; Lieber, C. M. Semiconductor nanowires: A platform for exploring limits and concepts for nano-enabled solar cells. *Energy Environ. Sci.* **2013**, *6*, 719–733.

[77] Liu, X. X.; Chao, D. L.; Su, D. P.; Liu, S. K.; Chen, L.; Chi, C. X.; Lin, J. Y.; Shen, Z. X.; Zhao, J. P.; Mai, L. et al. Graphene nanowires anchored to 3D graphene foam via self-assembly for high performance Li and Na ion storage. *Nano Energy* **2017**, *37*, 108–117.

[78] Kim, J.; Kim, M. S.; Lee, Y.; Kim, S. Y.; Sung, Y. E.; Ko, S. H. Hierarchically structured conductive polymer binders with silver nanowires for high-performance silicon anodes in lithium-ion batteries. *ACS Appl. Mater. Interfaces* **2022**, *14*, 17340–17347.

[79] Chockla, A. M.; Bogart, T. D.; Hessel, C. M.; Klavetter, K. C.; Mullins, C. B.; Korgel, B. A. Influences of gold, binder and electrolyte on silicon nanowire performance in li-ion batteries. *J. Phys. Chem. C* **2012**, *116*, 18079–18086.

[80] Chen, J. Y.; Zhou, W. X.; Chen, J.; Fan, Y.; Zhang, Z. Q.; Huang, Z. D.; Feng, X. M.; Mi, B. X.; Ma, Y. W.; Huang, W. Solution-processed copper nanowire flexible transparent electrodes with PEDOT: PSS as binder, protector and oxide-layer scavenger for polymer solar cells. *Nano Res.* **2015**, *8*, 1017–1025.

[81] Lee, S.; Jang, J.; Park, T.; Park, Y. M.; Park, J. S.; Kim, Y. K.; Lee, H. K.; Jeon, E. C.; Lee, D. K.; Ahn, B. et al. Electrodeposited silver nanowire transparent conducting electrodes for thin-film solar cells. *ACS Appl. Mater. Interfaces* **2020**, *12*, 6169–6175.

[82] Hong, X. S.; Wen, J. J.; Xiong, X. H.; Hu, Y. Y. Silver nanowire-carbon fiber cloth nanocomposites synthesized by UV curing adhesive for electrochemical point-of-use water disinfection. *Chemosphere* **2016**, *154*, 537–545.

[83] Jiang, X. C.; Herricks, T.; Xia, Y. N. CuO nanowires can be synthesized by heating copper substrates in air. *Nano Lett.* **2002**, *2*, 1333–1338.

[84] Xiang, L. J.; Guo, J.; Wu, C. H.; Cai, M. L.; Zhou, X. R.; Zhang, N. L. A brief review on the growth mechanism of CuO nanowires via thermal oxidation. *J. Mater. Res.* **2018**, *33*, 2264–2280.

[85] Huang, L. S.; Yang, S. G.; Li, T.; Gu, B. X.; Du, Y. W.; Lu, Y. N.; Shi, S. Z. Preparation of large-scale cupric oxide nanowires by thermal evaporation method. *J. Cryst. Growth* **2004**, *260*, 130–135.

[86] Hsieh, C. T.; Chen, J. M.; Lin, H. H.; Shih, H. C. Synthesis of well-ordered CuO nanofibers by a self-catalytic growth mechanism. *Appl. Phys. Lett.* **2003**, *82*, 3316–3318.
[87] Kumar, A.; Srivastava, A. K.; Tiwari, P.; Nandedkar, R. V. The effect of growth parameters on the aspect ratio and number density of CuO nanorods. *J. Phys. Condens. Matter* **2004**, *16*, 8531–8543.
[88] Kaur, M.; Muthe, K. P.; Despande, S. K.; Choudhury, S.; Singh, J. B.; Verma, N.; Gupta, S. K.; Yakhmi, J. V. Growth and branching of CuO nanowires by thermal oxidation of copper. *J. Cryst. Growth* **2006**, *289*, 670–675.
[89] Gonçalves, A. M. B.; Campos, L. C.; Ferlauto, A. S.; Lacerda, R. G. On the growth and electrical characterization of CuO nanowires by thermal oxidation. *J. Appl. Phys.* **2009**, *106*, 034303.
[90] Cao, F.; Jia, S. F.; Zheng, H.; Zhao, L. L.; Liu, H. H.; Li, L.; Zhao, L. G.; Hu, Y. M.; Gu, H. S.; Wang, J. B. Thermal-induced formation of domain structures in CuO nanomaterials. *Phys. Rev. Mater.* **2017**, *1*, 053401.
[91] Košiček, M.; Zavašnik, J.; Baranov, O.; Šetina Batič, B.; Cvelbar, U. Understanding the growth of copper oxide nanowires and layers by thermal oxidation over a broad temperature range at atmospheric pressure. *Cryst. Growth Des.* **2022**, *22*, 6656–6666.
[92] Zhang, Y. J.; Wang, N. L.; Gao, S. P.; He, R. R.; Miao, S.; Liu, J.; Zhu, J.; Zhang, X. A simple method to synthesize nanowires. *Chem. Mater.* **2002**, *14*, 3564–3568.
[93] Xu, C. H.; Yang, X. L.; Shi, S. Q.; Liu, Y.; Surya, C.; Woo, C. Effects of local gas-flow field on synthesis of oxide nanowires during thermal oxidation. *Appl. Phys. Lett.* **2008**, *92*, 253117.
[94] Huo, Z. Y.; Liu, H.; Yu, C. C. L.; Wu, Y. H.; Hu, H. Y.; Xie, X. Elevating the stability of nanowire electrodes by thin polydopamine coating for low-voltage electroporation-disinfection of pathogens in water. *Chem. Eng. J.* **2019**, *369*, 1005–1013.
[95] Zhou, J. F.; Wang, T.; Chen, W. S.; Lin, B. C.; Xie, X. Emerging investigator series: Locally enhanced electric field treatment (LEEFT) with nanowire-modified electrodes for water disinfection in pipes. *Environ. Sci. Nano* **2020**, *7*, 397–403.
[96] Hussain, I.; Ansari, M. Z.; Lamiel, C.; Hussain, T.; Javed, M. S.; Kaewmaraya, T.; Ahmad, M.; Qin, N.; Zhang, K. L. *In situ* grown heterostructure based on MOF-derived carbon containing n-type Zn-In-S and dry-oxidative p-type CuO as pseudocapacitive electrode materials. *ACS Energy Lett.* **2023**, *8*, 1887–1895.
[97] Hussain, I.; Iqbal, S.; Hussain, T.; Chen, Y. T.; Ahmad, M.; Javed, M. S.; Alfantazi, A.; Zhang, K. L. An oriented Ni-Co-MOF anchored on solution-free 1D CuO: A p-n heterojunction for supercapacitive energy storage. *J. Mater. Chem. A* **2021**, *9*, 17790–17800.
[98] Han, L. Y.; Li, H. Y.; Yang, L.; Liu, Y. L.; Liu, S. T. Rational design of $NiZn_x$@CuO nanoarray architectures for electrocatalytic oxidation of methanol. *ACS Appl. Mater. Interfaces* **2023**, *15*, 9392–9400.
[99] Fu, Y. Y.; Chen, J.; Zhang, H. Synthesis of Fe_2O_3 nanowires by oxidation of iron. *Chem. Phys. Lett.* **2001**, *350*, 491–494.
[100] Wang, D. W.; Zhu, B.; He, X.; Zhu, Z.; Hutchins, G.; Xu, P.; Wang, W. N. Iron oxide nanowire-based filter for inactivation of airborne bacteria. *Environ. Sci. Nano* **2018**, *5*, 1096–1106.
[101] Dlugosch, T.; Chnani, A.; Muralidhar, P.; Schirmer, A.; Biskupek, J.; Strehle, S. Thermal oxidation synthesis of crystalline iron-oxide nanowires on low-cost steel substrates for solar water splitting. *Semicond. Sci. Technol.* **2017**, *32*, 084001.
[102] Yin, Y.; Zhang, G.; Xia, Y. Synthesis and characterization of MgO nanowires through a vapor-phase precursor method. *Adv. Funct. Mater.* **2002**, *12*, 293–298.
[103] Liu, Y.; Zheng, C.; Wang, W.; Yin, C.; Wang, G. Synthesis and characterization of rutile SnO_2 nanorods. *Adv. Mater.* **2001**, *13*, 1883–1887
[104] Otnes, G.; Heurlin, M.; Graczyk, M.; Wallentin, J.; Jacobsson, D.; Berg, A.; Maximov, I.; Borgström, M. T. Strategies to obtain pattern fidelity in nanowire growth from large-area surfaces patterned using nanoimprint lithography. *Nano Res.* **2016**, *9*, 2852–2861
[105] Tuzluca, F. N.; Yesilbag, Y. O.; Ertugrul, M. Synthesis of In_2O_3 nanostructures with different morphologies as potential supercapacitor electrode materials. *Appl. Surf. Sci.* **2018**, *427*, 956–964.
[106] Gohier, A.; Laïk, B.; Pereira-Ramos, J. P.; Cojocaru, C. S.; Tran-Van, P. Influence of the diameter distribution on the rate capability of silicon nanowires for lithium-ion batteries. *J. Power Sources* **2012**, *203*, 135–139.
[107] Tuzluca, F. N.; Yesilbag, Y. O.; Ertugrul, M. Investigation of temperature, catalyst thickness and substrate effects in In_2O_3 nanostructures. *J. Phys. Chem. Solids* **2017**, *111*, 439–446.
[108] Storan, D.; Ahad, S. A.; Forde, R.; Kilian, S.; Adegoke, T. E.; Kennedy, T.; Geaney, H.; Ryan, K. M. Silicon nanowire growth on carbon cloth for flexible Li-ion battery anodes. *Mater. Today Energy* **2022**, *27*, 101030.
[109] Collins, G. A.; Kilian, S.; Geaney, H.; Ryan, K. M. A nanowire nest structure comprising copper silicide and silicon nanowires for lithium-ion battery anodes with high areal loading. *Small* **2021**, *17*, 2102333.
[110] Tuzluca, F. N.; Yesilbag, Y. O.; Ertugrul, M. Synthesis of ultra-long boron nanowires as supercapacitor electrode material. *Appl. Surf. Sci.* **2019**, *493*, 787–794.
[111] Breuer, S.; Pfüller, C.; Flissikowski, T.; Brandt, O.; Grahn, H. T.; Geelhaar, L.; Riechert, H. Suitability of Au- and self-assisted GaAs nanowires for optoelectronic applications. *Nano Lett.* **2011**, *11*, 1276–1279.
[112] Joyce, H. J.; Gao, Q.; Hoe Tan, H.; Jagadish, C.; Kim, Y.; Zou, J.; Smith, L. M.; Jackson, H. E.; Yarrison-Rice, J. M.; Parkinson, P. et al. III-V semiconductor nanowires for optoelectronic device applications. *Prog. Quantum Electron.* **2011**, *35*, 23–75.
[113] Duan, X. F.; Huang, Y.; Cui, Y.; Wang, J. F.; Lieber, C. M. Indium phosphide nanowires as building blocks for nanoscale electronic and optoelectronic devices. *Nature* **2001**, *409*, 66–69.
[114] Dayeh, S. A.; Aplin, D. P. R.; Zhou, X. T.; Yu, P. K. L.; Yu, E. T.; Wang, D. L. High electron mobility InAs nanowire field-effect transistors. *Small* **2007**, *3*, 326–332
[115] Pi, S. Y.; Sun, M. Y.; Zhao, Y. F.; Chong, Y. X.; Chen, D.; Liu, H. Electroporation-coupled electrochemical oxidation for rapid and efficient water disinfection with Co_3O_4 nanowire arrays-modified graphite felt electrodes. *Chem. Eng. J.* **2022**, *435*, 134967
[116] Liu, H.; Huang, W.; Yu, Y.; Chen, D. Lightning-rod effect on nanowire tips reinforces electroporation and electrochemical oxidation: An efficient strategy for eliminating intracellular antibiotic resistance genes. *ACS Nano* **2023**, *17*, 3037–3046.
[117] Lu, Y. W.; Liang, X. X.; Wang, C. Y.; Chen, D.; Liu, H. Synergistic nanowire-assisted electroporation and chlorination for inactivation of chlorine-resistant bacteria in drinking water systems via inducing cell pores for chlorine permeation. *Water Res.* **2023**, *229*, 119399
[118] Wang, M. M.; Liu, L. J.; Wen, J. T.; Ding, Y.; Xi, J. R.; Li, J. C.; Lu, F. Z.; Wang, W. K.; Xu, J. Multimetallic CuCoNi oxide nanowires *in situ* grown on a nickel foam substrate catalyze persulfate activation via mediating electron transfer. *Environ. Sci. Technol.* **2022**, *56*, 12613–12624.
[119] Zhao, H. M.; Zhang, Z. P.; Zhou, C. G.; Zhang, H. F. Tuning the morphology and size of $NiMoO_4$ nanosheets anchored on $NiCo_2O_4$ nanowires: The optimized core–shell hybrid for high energy density asymmetric supercapacitors. *Appl. Surf. Sci.* **2021**, *541*, 148458.
[120] Zhou, X. Y.; Chen, G. H.; Tang, J. J.; Ren, Y. P.; Yang, J. One-dimensional $NiCo_2O_4$ nanowire arrays grown on nickel foam for high-performance lithium-ion batteries. *J. Power Sources* **2015**, *299*, 97–103.
[121] Zhao, M. X.; Yang, L. Q.; Cai, Z. Y.; Guo, H.; Zhao, Z. J. Design of binder-free hierarchical Mo-Fe-Ni phosphides nanowires array anchored on carbon cloth with high electrocatalytic capability toward hydrogen evolution reaction. *J. Alloys Compd.* **2022**, *891*, 162064.
[122] Zhou, W. J.; Liu, X. J.; Sang, Y. H.; Zhao, Z. H.; Zhou, K.; Liu, H.; Chen, S. W. Enhanced performance of layered titanate nanowire-based supercapacitor electrodes by nickel ion exchange. *ACS Appl. Mater. Interfaces* **2014**, *6*, 4578–4586.
[123] Wang, C. J.; Liu, X. J.; Sang, Y. H.; Zhao, Z. H.; Zhou, K.; Liu, H.; Chen, S. W. Fabrication and shell optimization of synergistic TiO_2-

MoO_3 core–shell nanowire array anode for high energy and power density lithium-ion batteries. *Adv. Funct. Mater.* **2015**, *25*, 3524–3533.

[124] Lu, Y. W.; Wang, Y.; Liu, Y. R.; Liu, H. Square-wave alternating voltage driving promotes nanowire-assisted electroporation inactivation and fouling resistance of pathogenic bacteria for water disinfection. *Chem. Eng. J.* **2024**, *480*, 148074.

[125] Wang, Y.; Lu, Y. W.; Liu, H. Nanowire electroporation-induced cell pores on antibiotic-resistant bacteria to promote chlorine permeation for eliminating intracellular antibiotic resistance genes. *Chem. Eng. J.* **2024**, *479*, 147801.

[126] Wang, H. B.; Desbordes, M.; Xiao, Y.; Kubo, T.; Tada, K.; Bessho, T.; Nakazaki, J.; Segawa, H. Highly stable interdigitated PbS quantum dot and ZnO nanowire solar cells with an automatically embedded electron-blocking layer. *ACS Appl. Energy Mater.* **2021**, *4*, 5918–5926.

[127] Lin, Y. C.; Liu, S. Robust ZnO nanowire photoanodes with oxygen vacancies for efficient photoelectrochemical cathodic protection. *Appl. Surf. Sci.* **2021**, *566*, 150694.

[128] Lee, W.; Park, S. J. Porous anodic aluminum oxide: Anodization and templated synthesis of functional nanostructures. *Chem. Rev.* **2014**, *114*, 7487–7556.

[129] Kim, K.; Kim, M.; Cho, S. M. Pulsed electrodeposition of palladium nanowire arrays using AAO template. *Mater. Chem. Phys.* **2006**, *96*, 278–282.

[130] Schiavi, P. G.; Altimari, P.; Rubino, A.; Pagnanelli, F. Electrodeposition of cobalt nanowires into alumina templates generated by one-step anodization. *Electrochim. Acta* **2018**, *259*, 711–722.

[131] Guiliani, J.; Cadena, J.; Monton, C. Template-assisted electrodeposition of Ni and Ni/Au nanowires on planar and curved substrates. *Nanotechnology* **2018**, *29*, 075301.

[132] Michalska-Domańska, M.; Norek, M.; Stępniowski, W. J.; Budner, B. Fabrication of high quality anodic aluminum oxide (AAO) on low purity aluminum—A comparative study with the AAO produced on high purity aluminum. *Electrochim. Acta* **2013**, *105*, 424–432.

[133] Weng, W.; Xiao, W. Electrodeposited silicon nanowires from silica dissolved in molten salts as a binder-free anode for lithium-ion batteries. *ACS Appl. Energy Mater.* **2019**, *2*, 804–813.

[134] Li, W. G.; Tekell, M. C.; Liu, C.; Hethcock, J. A.; Fan, D. L. Flexible all-solid-state supercapacitors of high areal capacitance enabled by porous graphite foams with diverging microtubes. *Adv. Funct. Mater.* **2018**, *28*, 1800601.

[135] Luo, X. F.; Li, W. G.; Liang, Z. X.; Liu, Y. F.; Fan, D. E. Portable bulk-water disinfection by live capture of bacteria with divergently branched porous graphite in electric fields. *ACS Nano* **2023**, *17*, 10041–10054.

[136] Tang, J. X.; Tian, N.; Xiao, L. P.; Chen, Q. S.; Wang, Q.; Zhou, Z. Y.; Sun, S. G. Helical PdPtAu nanowires bounded with high-index facets selectively switch the pathway of ethanol electrooxidation. *J. Mater. Chem. A* **2022**, *10*, 10902–10908.

[137] Tang, J. X.; Chen, Q. S.; You, L. X.; Liao, H. G.; Sun, S. G.; Zhou, S. G.; Xu, Z. N.; Chen, Y. M.; Guo, G. C. Screw-like PdPt nanowires as highly efficient electrocatalysts for methanol and ethylene glycol oxidation. *J. Mater. Chem. A* **2018**, *6*, 2327–2336.

[138] Dai, X. C.; Hou, S.; Huang, M. H.; Li, Y. B.; Li, T.; Xiao, F. X. Electrochemically anodized one-dimensional semiconductors: A fruitful platform for solar energy conversion. *J. Phys. Energy* **2019**, *1*, 022002.

[139] Roy, P.; Berger, S.; Schmuki, P. TiO_2 nanotubes: Synthesis and applications. *Angew. Chem., Int. Ed.* **2011**, *50*, 2904–2939.

[140] Zhang, Z. H.; Hossain, M. F.; Takahashi, T. Fabrication of shape-controlled α-Fe_2O_3 nanostructures by sonoelectrochemical anodization for visible light photocatalytic application. *Mater. Lett.* **2010**, *64*, 435–438.

[141] LaTempa, T. J.; Feng, X. J.; Paulose, M.; Grimes, C. A. Temperature-dependent growth of self-assembled hematite (α-Fe_2O_3) nanotube arrays: Rapid electrochemical synthesis and photoelectrochemical properties. *J. Phys. Chem. C* **2009**, *113*, 16293–16298.

[142] Huo, Z. Y.; Zhou, J. F.; Wu, Y. T.; Wu, Y. H.; Liu, H.; Liu, N.; Hu, H. Y.; Xie, X. A Cu_3P nanowire enabling high-efficiency, reliable, and energy-efficient low-voltage electroporation-inactivation of pathogens in water. *J. Mater. Chem. A* **2018**, *6*, 18813–18820

[143] Huo, Z. Y.; Liu, H.; Wang, W. L.; Wang, Y. H.; Wu, Y. H.; Xie, X.; Hu, H. Y. Low-voltage alternating current powered polydopamine-protected copper phosphide nanowire for electroporation-disinfection in water. *J. Mater. Chem. A* **2019**, *7*, 7347–7354.

[144] Su, P. F.; Zhang, Z. Q.; Luo, L. S.; Zhang, Z. Y.; Lan, C. F.; Li, Y. H.; Xu, S. W.; Pei, S. P.; Lin, G. Y.; Li, C. et al. Cu nanowire array with designed interphases enabling high performance Si anode toward flexible lithium-ion battery. *Nano Res.* **2024**, *17*, 1516–1524.

[145] Mateen Tantray, A.; Shah, M. A. Photo electrochemical ability of dense and aligned ZnO nanowire arrays fabricated through electrochemical anodization. *Chem. Phys. Lett.* **2020**, *747*, 137346.

[146] Tello, A.; Boulett, A.; Sánchez, J.; Pizarro, G. D. C.; Soto, C.; Linarez Pérez, O. E.; Sanhueza, R.; Oyarzún, D. P. An unexplored strategy for synthesis of ZnO nanowire films by electrochemical anodization using an organic-based electrolyte. Morphological and optical properties characterization. *Chem. Phys. Lett.* **2021**, *778*, 138825.

[147] Zhang, W.; Wen, X.; Yang, S.; Berta, Y.; Wang, Z. L. Single-crystalline scroll-type nanotube arrays of copper hydroxide synthesized at room temperature. *Adv. Mater.* **2003**, *15*, 822–825.

[148] Huo, Z. Y.; Yang, Y. X.; Jeong, J. M.; Wang, X. X.; Zhang, H.; Wei, M. D.; Dai, K. R.; Xiong, P. X.; Kim, S. W. Self-powered disinfection using triboelectric, conductive wires of metal-organic frameworks. *Nano Lett.* **2023**, *23*, 3090–3097.

[149] Chen, F.; Chen, C.; Hu, Q.; Xiang, B.; Song, T. T.; Zou, X. F.; Li, W. N.; Xiong, B. X.; Deng, M. S. Synthesis of CuO@CoNi LDH on Cu foam for high-performance supercapacitors. *Chem. Eng. J.* **2020**, *401*, 126145.

[150] Çakır, O. Review of etchants for copper and its alloys in wet etching processes. *Key Eng. Mater.* **2008**, 364–366, 460–465

[151] Yue, L. F.; Chen, S. G.; Wang, S. T.; Wang, C. Y.; Hao, X. P.; Cheng, Y. F. Water disinfection using Ag nanoparticle-CuO nanowire co-modified 3D copper foam nanocomposites in high flow under low voltages. *Environ. Sci. Nano* **2019**, *6*, 2801–2809.

[152] Wang, S. T.; Dong, L. T.; Zhang, M. T.; Cheng, F.; Chen, S. G. N-doped carbon-coated Cu_2O nanowire arrays on copper foam for rapid and stable water disinfection. *J. Colloid Interface Sci.* **2022**, *625*, 761–773.

[153] Lu, C. H.; Qi, L. M.; Yang, J. H.; Tang, L.; Zhang, D. Y.; Ma, J. M. Hydrothermal growth of large-scale micropatterned arrays of ultralong ZnO nanowires and nanobelts on zinc substrate. *Chem. Commun.* **2006**, 3551–3553

[154] Luo, W.; Zhang, Q.; Zhang, J.; Moioli, E.; Zhao, K.; Züttel, A. Electrochemical reconstruction of ZnO for selective reduction of CO_2 to CO. *Appl. Catal. B Environ.* **2020**, *273*, 119060.

[155] Li, X. L. Metal assisted chemical etching for high aspect ratio nanostructures: A review of characteristics and applications in photovoltaics. *Curr. Opin. Solid State Mater. Sci.* **2012**, *16*, 71–81.

[156] Huang, Z. P.; Geyer, N.; Werner, P.; De Boor, J.; Gösele, U. Metal-assisted chemical etching of silicon: A review. *Adv. Mater.* **2011**, *23*, 285–308.

[157] Leonardi, A. A.; Faro, M. J. L.; Irrera, A. Silicon nanowires synthesis by metal-assisted chemical etching: A review. *Nanomaterials* **2021**, *11*, 383.

[158] Dimova-Malinovska, D.; Sendova-Vassileva, M.; Tzenov, N.; Kamenova, M. Preparation of thin porous silicon layers by stain etching. *Thin Solid Films* **1997**, *297*, 9–12.

[159] Li, X.; Bohn, P. W. Metal-assisted chemical etching in HF/H_2O_2 produces porous silicon. *Appl. Phys. Lett.* **2000**, *77*, 2572–2574.

[160] Chang, S. W.; Chuang, V. P.; Boles, S. T.; Ross, C. A.; Thompson, C. V. Densely packed arrays of ultra-high-aspect-ratio silicon nanowires fabricated using block-copolymer lithography and metal-assisted etching. *Adv. Funct. Mater.* **2009**, *19*, 2495–2500.

[161] Yae, S.; Kawamoto, Y.; Tanaka, H.; Fukumuro, N.; Matsuda, H. Formation of porous silicon by metal particle enhanced chemical

etching in HF solution and its application for efficient solar cells. *Electrochem. Commun.* **2003**, *5*, 632–636.

[162] Huang, Z. P.; Zhang, X. X.; Reiche, M.; Liu, L. F.; Lee, W.; Shimizu, T.; Senz, S.; Gösele, U. Extended arrays of vertically aligned sub-10 nm diameter [100] Si nanowires by metal-assisted chemical etching. *Nano Lett.* **2008**, *8*, 3046–3051.

[163] Pérez-Díaz, O.; Quiroga-González, E.; Hansen, S.; Silva-González, N. R.; Carstensen, J.; Adelung, R. Fabrication of silicon microwires by a combination of chemical etching steps and their analysis as anode material in Li-ion batteries. *Mater. Technol.* **2019**, *34*, 785–791.

[164] Yeom, J.; Ratchford, D.; Field, C. R.; Brintlinger, T. H.; Pehrsson, P. E. Decoupling diameter and pitch in silicon nanowire arrays made by metal-assisted chemical etching. *Adv. Funct. Mater.* **2014**, *24*, 106–116.

[165] Mishra, S. M.; Dey, S.; Singha, T.; Mandal, S.; Dehury, A. K.; Chaudhary, Y. S.; Satpati, B. Enhanced optical properties and dark *I–V* characteristics of silicon nanowire-carbon quantum dots heterostructures. *Mater. Res. Bull.* **2023**, *164*, 112262.

[166] Um, H. D.; Kim, N.; Lee, K.; Hwang, I.; Hoon Seo, J.; Yu, Y. J.; Duane, P.; Wober, M.; Seo, K. Versatile control of metal-assisted chemical etching for vertical silicon microwire arrays and their photovoltaic applications. *Sci. Rep.* **2015**, *5*, 11277.

[167] Assa Aravindh, S.; Xin, B.; Mitra, S.; Roqan, I. S.; Najar, A. GaN and InGaN nanowires prepared by metal-assisted electroless etching: Experimental and theoretical studies. *Results Phys.* **2020**, *19*, 103428.

[168] Najar, A.; Shafa, M.; Anjum, D. Synthesis, optical properties and residual strain effect of GaN nanowires generated via metal-assisted photochemical electroless etching. *RSC Adv.* **2017**, *7*, 21697–21702.

[169] Soopy, A. K. K.; Najar, A.; Ravau, F.; Anjum, D. H. Facile development of InP nanowires via metal-assisted chemical etching and their optical properties. In *2021 6th International Conference on Renewable Energy: Generation and Applications* (*ICREGA*) **2021**, pp, 25–28

[170] Zhao, S. F.; Han, F.; Li, J. H.; Meng, X. Y.; Huang, W. P.; Cao, D. X.; Zhang, G. P.; Sun, R.; Wong, C.-P. Advancements in copper nanowires: Synthesis, purification, assemblies, surface modification, and applications, *Small* **2018**, *14*, 1800047.

[171] Humphreys, F. J.; Hatherly, M. *Recrystallization and Related Annealing Phenomena; Elsevier*: Amsterdam, **2018**.

[172] Cudennec, Y.; Lecerf, A. The transformation of $Cu(OH)_2$ into CuO, revisited. *Solid State Sci.* **2003**, *5*, 1471–1474.

[173] Huang, H. W.; Yu, Q.; Ye, Y. H.; Wang, P.; Zhang, L. Q.; Gao, M. X.; Peng, X. S.; Ye, Z. Z. Thin copper oxide nanowires/carbon nanotubes interpenetrating networks for lithium ion batteries. *CrystEngComm* **2012**, *14*, 7294–7300.

[174] Qiao, H. D.; Yu, Y. W.; Song, K. F.; Liu, Z. Y.; Hu, X. L. High mass loading NiCo-OH nanothorns coated CuO nanowire arrays for high-capacity nickel-zinc battery. *Nanotechnology* **2021**, *32*, 505404.

[175] Shi, Y. M.; Zhang, B. Recent advances in transition metal phosphide nanomaterials: Synthesis and applications in hydrogen evolution reaction. *Chem. Soc. Rev.* **2016**, *45*, 1529–1541.

[176] Xu, X. D.; Liu, W.; Kim, Y.; Cho, J. Nanostructured transition metal sulfides for lithium ion batteries: Progress and challenges. *Nano Today* **2014**, *9*, 604–630.

[177] Harris, S.; Chianelli, R. R. Catalysis by transition metal sulfides: A theoretical and experimental study of the relation between the synergic systems and the binary transition metal sulfides. *J. Catal.* **1986**, *98*, 17–31.

[178] Suen, N. T.; Hung, S. F.; Quan, Q.; Zhang, N.; Xu, Y. J.; Chen, H. M. Electrocatalysis for the oxygen evolution reaction: Recent development and future perspectives. *Chem. Soc. Rev.* **2017**, *46*, 337–365.

[179] Zhou, W. J.; Liu, H.; Boughton, R. I.; Du, G. J.; Lin, J. J.; Wang, J. Y.; Liu, D. One-dimensional single-crystalline Ti-O based nanostructures: Properties, synthesis, modifications and applications. *J. Mater. Chem.* **2010**, *20*, 5993–6008

[180] Britvin, S. N.; Lotnyk, A.; Kienle, L.; Krivovichev, S. V.; Depmeier, W. Layered hydrazinium titanate: Advanced reductive adsorbent and chemical toolkit for design of titanium dioxide nanomaterials. *J. Am. Chem. Soc.* **2011**, *133*, 9516–9525.

[181] Kang, Q.; Vernisse, L.; Remsing, R. C.; Thenuwara, A. C.; Shumlas, S. L.; Mckendry, I. G.; Klein, M. L.; Borguet, E.; Zdilla, M. J.; Strongin, D. R. Effect of interlayer spacing on the activity of layered manganese oxide bilayer catalysts for the oxygen evolution reaction. *J. Am. Chem. Soc.* **2017**, *139*, 1863–1870.

[182] Zhang, L.; Zhang, Q.; Li, J. Layered titanate nanosheets intercalated with myoglobin for direct electrochemistry. *Adv. Funct. Mater.* **2007**, *17*, 1958–1965.

[183] García-García, P.; Müller, M.; Corma, A. MOF catalysis in relation to their homogeneous counterparts and conventional solid catalysts. *Chem. Sci.* **2014**, *5*, 2979–3007.